

Computer Chemistry

Analysis of Proton NMR in Hydrogen Bonds in Terms of Lone-Pair and Bond Orbital Contributions

Kiplangat Sutter,^[a] Gustavo A. Aucar,^[b] and Jochen Autschbach*^[a]

Abstract: NMR spectroscopic parameters of the proton involved in hydrogen bonding are studied theoretically. The set of molecules includes systems with internal resonance-assisted hydrogen bonds, internal hydrogen bonds but no resonance stabilization, the acetic acid dimer (AAD), a DNA base pair, and the hydrogen succinate anion (HSA). Ethanol and guanine represent reference molecules without hydrogen bonding. The calculations are based on zero-point vibrationally averaged molecular structures in order to include anharmonicity effects in the NMR parameters. An analysis of the calculated NMR shielding and J -coupling is performed in terms of "chemist's orbitals", that is, localized molecular orbitals (LMOs) representing lone-pairs, atomic cores, and bonds.

The LMO analysis quantitatively connects the strong deshielding of the protons in resonance-assisted hydrogen bonds with delocalization involving the π -backbone. Resonance is also shown to be an important factor causing deshielding of the OH protons for AAD and HSA, but not for the DNA base pair. Nitromalonamide (NMA) and HSA have particularly strong hydrogen bonds exhibiting signs of covalency in the associated J -couplings. The analysis results show how NMR spectroscopic parameters that are characteristic for hydrogen bonded protons are influenced by the geometry and degree of covalency of the hydrogen bond as well as intra- and intermolecular resonance.

Introduction

Hydrogen bonding (H-bonding) is of tremendous importance and interest in chemistry and biochemistry. There are various experimental techniques available for the study of H-bonds. Among those techniques is NMR spectroscopy, which is also among the most frequently applied all-around spectroscopic tools available to chemists. Hydrogen-bonding of protons manifests itself in important characteristics of NMR chemical shifts and J -couplings.^[1–3] Accepted experimental evidence for H-bonding is a pronounced NMR de-shielding of the respective proton and the presence of J -coupling through hydrogen bonds,^[4–10] along with nuclear Overhauser enhancements. The de-shielding is particularly pronounced for low-barrier H-bonds.^[11] From a theoretical perspective, there are many different ways of analyzing and characterizing hydrogen bonds, such as interaction energy decompositions, natural bond orbital (NBO) methods, and atoms-in-molecules (AIM) electron density topology analyses.

For overviews and in particular a discussion of the covalent character of hydrogen bonds see, for instance, references [12] and [13]. NMR J -coupling has been used to assess the extent of covalency in H-bonds.^[8] The proton shielding has also been investigated theoretically in relation to covalency within the H-bond participants.^[14]

A strong de-shielding of a H-bonded proton may be thought of as being caused by a loss of electron density, or by the H-bond promoting a particularly effective induction of paramagnetic current-density by the external magnetic field,^[15] or a combination of these effects.^[16,17] The scales for the absolute NMR shielding constant σ_N for a given isotope N (such as the H-bonded proton) and the chemical shift δ_N have opposite directions due to the definition of the shift via the resonance frequencies. To a very good approximation for light nuclei, $\delta_N^{\text{probe}} = \sigma_N^{\text{ref}} - \sigma_N^{\text{probe}}$, where σ_N^{ref} is the shielding constant of isotope N in the reference compound. It has recently been demonstrated that the absolute shielding can be measured directly by NMR spectroscopy.^[18,19] The proton absolute shielding scale is well established, with a tetramethylsilane (TMS) proton shielding of 33.480(5) ppm for 1% TMS in CDCl₃ at 300 K.^[19] In a H-bond, the shielding is moderately to severely reduced. A strong de-shielding relative to TMS translates to a large positive chemical shift.

As an example, malonaldehyde (MA) and related compounds in their enol tautomeric forms afford an intramolecular hydrogen bond within a planar, partially π -conjugated, 6-membered quasi-heterocycle, shown in Figure 1 among the other molecules studied herein. The chemical shift of the H-bonded

[a] K. Sutter, J. Autschbach

■ Please give academic titles for all authors ■ Department of Chemistry, University at Buffalo State University of New York
Buffalo, NY 14260-3000 (USA)
E-mail: jochena@buffalo.edu

[b] G. A. Aucar

Physics Department of the Natural and Exact Science Faculty
Northeastern University of Argentina and IMIT Institute
CONICET-UNNE, Av. Libertad 5500, W 3404 AAS Corrientes (Argentina)

Supporting information for this article is available on the WWW under <http://dx.doi.org/10.1002/chem.201502346>. Including the full references for Gaussian 09 and the Amsterdam density functional suite; additional LMO plots; additional NMR spectroscopy data; optimized and zero-point averaged effective structures for all molecules.

proton in MA is $\delta = 14$ ppm^[20] and therefore the proton is much more de-shielded than hydrogen atoms in the majority of diamagnetic organic compounds. The enol form of pentane-2,4-dione (acetylacetonate, PD in Figure 1) affords a similarly strongly de-shielded H-bonded proton as MA, with δ around 15 ppm.^[21,15] Related derivatives cover a chemical shift range of 13–17 ppm.^[21] The distinct NMR parameters of the enol versus keto forms of such compounds find frequent use in undergraduate laboratory experiments set up to study the tautomer equilibrium, and its solvent dependence, by NMR spectroscopy.^[22] An interesting related system is 2-hydroxyacetophenone, where a C=C bond is in conjugation with an H-bonding carbonyl group but also part of an aromatic 6-membered ring; the chemical shift of the OH proton is 12 ppm.^[23] A very large proton shift exceeding 20 ppm has been found for the internal H-bond of the hydrogen succinate anion (HSA), a partially deprotonated dicarboxylic acid, and related systems.^[24] Large proton shifts of 12 ppm and above are also found for intermolecular hydrogen bonds, such as for O...H in carboxylic acid dimers or N...H in DNA base pairs.^[25] For the former, a strong dependence of the proton shifts on the O–H distances has been noted.^[26] Reference [26] and other studies by

Limbach and co-workers noted a very good correlation between the distance (d) difference $D_{\text{OHO}} = (r_{\text{O}\cdots\text{H}} - r_{\text{O}\cdots\text{H}})/2$ and the ¹H NMR shifts in O–H...O hydrogen bond environments.^[27,24] Furthermore, H/D isotope effects on other chemical shifts in the vicinity of the H-bond,^[24,26,28–33] such as ¹³C, can be indicators of the average hydrogen positions. See also reference [34].

Strong H-bonding with concomitant small D_{XHX} (typically X = O, N) is driven by the overall energetics of a system. For example, for β -dicarbonyl compounds such as MA there is the concept of a resonance-assisted hydrogen bond (RAHB).^[35] RAHB is a cooperative effect of the hydrogen bond and the π -system in the backbone. Regarding the relationship between π -delocalization in the neighborhood of H-bonds see also reference [36]. A somewhat related discussion in reference [37] focuses on charge-assisted H-bonding^[12] in complexes with N–H...Cl, B–H...Br and P–H...Cl type of interactions. The RAHB effect has received considerable attention. For MA and related compounds^[38] it was found that breaking/deactivating the π conjugation would weaken the strength of the H-bond. However, little changes on the topological properties of the electron densities were seen. Reference [39] also featured a topological

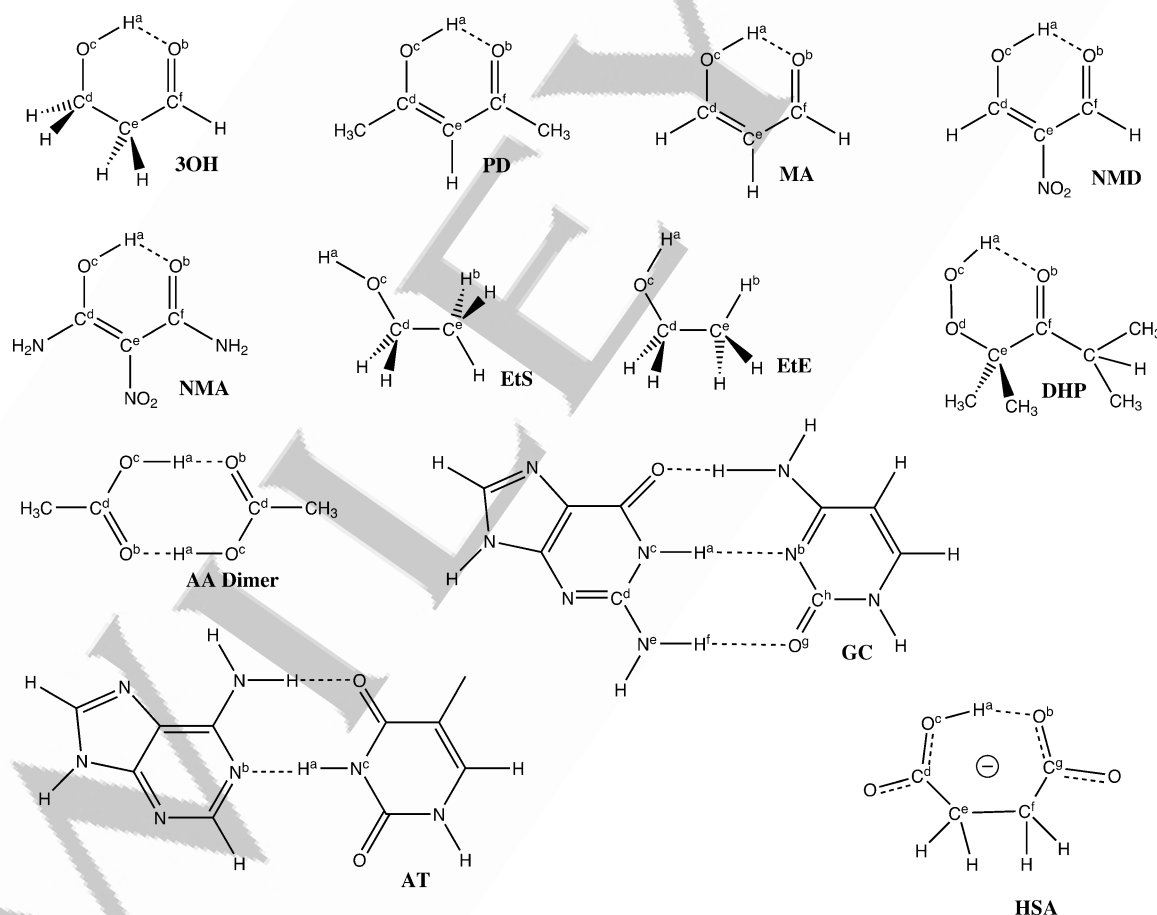


Figure 1. Molecules studied herein, and atom labels: 3OH = 3-hydroxypropanal; PD = 2,4-pentanedione, MA = malonaldehyde; NMD = nitromalonaldehyde; NMA = nitromalonamide; EtS = ethanol in a staggered conformation; EtE = eclipsed form of ethanol and with OH *cis* to C–C; DHP = 2,4-dimethyl-2-hydroperoxy-3-pentanone; AAD = acetic acid dimer, GC = guanine (G) and cytosine (C) DNA base-pair, AT = adenine (A) and thymine (T) base-pair, HSA = hydrogen succinate anion. Note that guanine not included in this list is G = guanine (similar to the G in GC). Detailed shielding and J -coupling LMO analyses were performed for all molecules except PD, EtS, and AT.

density study, along with a natural bond orbital (NBO)^[40] based analysis. A related computational study of substituted β -dicarbonyl compounds can be found in reference [41], which also correlated calculated NMR shifts with the extent of resonance stabilization. Reference [42] confirmed the influence of the π system on the hydrogen bond of MA and its derivatives using a polarizability analysis based on localized orbitals within a polarization propagator approach. In a recent paper,^[16] one of us studied NMR chemical shifts and J -coupling constants for MA and various derivatives. Relatively large contributions of non-contact mechanisms to J -couplings through H-bonds were found for systems within the RAHB category.

In this present work, we aim more generally at uncovering explicit links between NMR parameters related to hydrogen bonding and a chemically intuitive picture of bonding obtained directly from quantum chemical calculations. To this end, the proton NMR shielding and the electron-mediated (indirect) nuclear spin–spin coupling constants (J -couplings) between the H-bonded protons and oxygen atoms or nitrogen atoms in the H-bond as well as more distant atoms are analyzed in terms of quantitative contributions from “chemist’s” bonds and lone pair orbitals. These are represented quantum mechanically by localized molecular orbitals (LMOs) and—for the purpose of this study—obtained from density functional theory (DFT). The analysis tools were originally developed by us to study NMR parameters of heavy metal complexes,^[17,43–45] but they are applicable to all elements from the periodic table, light or heavy. The general utility of localized lone-pair and bond orbitals in the study of NMR parameters has been amply demonstrated; for selected examples see references [17,46–52]. Our LMO analysis includes the effects from paramagnetic and diamagnetic ring currents and spin densities induced by the external fields and the nuclear spin magnetic moments, per orbital, and does not introduce approximations beyond those introduced by the underlying DFT calculation. To our knowledge, such techniques have not yet been applied to study the NMR parameters of H-bonded protons in detail. The effects from H-bonding on the proton NMR parameters are in this work explicitly quantified in terms of contributions to the proton shielding and to one-bond J -couplings involving the proton, for instance, from the lone-pairs (LPs) of the H-bonding partner $X=N, O$, the LP orbitals of the $X-H$ heteroatom, the $X-H$ σ bond, π bonds in the backbone of RAHB systems, and other bonding or LP orbitals in the molecules.

Among the questions that are addressed in this work are: 1) Do the proton NMR shielding and J -coupling analyses reveal information about covalency within the H-bond moiety? 2) Does resonance in an RAHB directly show up in the analysis, or are the NMR parameters primarily a function of D_{XH} without explicit resonance contributions in the NMR parameters; 3) Does resonance play a role for other strong H-bonds that do not fall in the RAHB category; 4) does an analysis reveal clear distinctions or similarities between NMA and HSA (Figure 1), which exhibit the strongest proton de-shielding among our samples? NMA belongs in the RAHB category, HSA does not but it is negatively charged. 5) Does the analysis reveal qualitative differences between $O-H\cdots O$ versus $N-H\cdots N$ hydrogen

bonds and is there evidence for RAHB in the NMR analysis of a DNA base pair? The analysis data are compared to ethanol in gas phase, representing an $O-H$ proton that is not involved in a H-bond, and to guanine as a representative of an $N-H$ proton without hydrogen bonding. Among our findings is that signs and magnitudes of the J -couplings correlate well with the degree of covalent interactions between H and X, and, importantly, the LMO analysis implicates the same bonds and lone pairs that drive the chemical shift trends. Further, resonance plays an important role not only for RAHB systems. The analysis technique is easily transferable to H-bonds in other types of molecules, highlighting the insight that can be gained from studying NMR parameters with chemically intuitive, yet quantitative, techniques rooted in first-principles theory.

Computational Details

For 3 OH, MA, NMD, and NMA, optimized B3LYP/6-311++G** geometries were taken from Zarycz et al.^[16] and used without further optimization. Structures for the other systems were optimized with B3LYP/6-311++G** using Gaussian 09.^[53] Most NMR computations utilized a 2012 developer’s version of Amsterdam density functional (ADF) package^[54] incorporating the NMR shielding and J -coupling LMO analysis modules.^[17,43–45] J -coupling constants and NMR nuclear shielding tensors were calculated with the hybrid functional PBE0,^[55,56] using triple- ζ polarized (TZP) Slater-type orbital (STO) all-electron basis sets. Shielding tensors were visualized as described in reference [57]. Vibrational averages of shielding constants and effective zero-point vibrationally (ZPV) averaged molecular structures were obtained with a numerical differentiation code described in reference [58]. Due to the better performance of the numerical integration grids available with Gaussian for finite-difference calculations of shielding derivatives and cubic force constants, the ZPV averages were calculated with G09 with B3LYP/6-311++G** for the force constants and effective geometries, and PBE0/cc-pVTZ for NMR shielding. As shown in Table S1 in the Supporting Information, shielding constants obtained with the Gaussian-type orbital (GTO) basis cc-pVTZ agree well with those obtained with ADF and the TZP STO basis. The xyz coordinates for the equilibrium and ZPV effective geometries are provided in the Supporting Information. Additional ZPV averaged data were generated for MA and NMA for a deuterated H-bond (Table S9 in the Supporting Information), to demonstrate the magnitude of the isotope effects for two representative cases. We decided to forego additional ZPV calculations for the remaining systems due to the significant computational cost.

LMOs were generated at the PBE0/TZP level using the natural bond orbital (NBO) algorithms^[40] of the NBO 5.0 program^[59] available in the ADF package. The NMR analyses in terms of “natural” LMOs (NLMOs) were performed with the effective geometries, using the techniques described in references [43,45,60,61]. As explained in reference [45], the analysis of a J -coupling constant involving nuclei N and M is given as an average of the LMO contributions from two independent calculations, one in which the nuclear spin magnetic moment of N is used as the perturbation when solving the coupled-perturbed Kohn–Sham equations, and one where the magnetic moment of nucleus M is used. This protocol ensures that equivalent LMOs contribute equally to the results.

Results and Discussion

Figure 1 shows the systems investigated in this work, along with the adopted atom labeling as well as shortcuts names for the molecules. The atom labeling within the hydrogen bond moieties is $X^c-H^a...X^b$ and the same for all molecules, meaning that H^a is the proton of the XH ($X=N, O$) group for which the NMR shift is analyzed, X^c is the heteroatom of the same group, and X^b is the heteroatom H-bonding to H^a .

Bond orders

We first discuss the extent of covalency of the various H-bonds as quantified by calculated bond indices. Selected Wiberg bond indices (WBIs)^[62,63] involving H^a are collected in Table 1. The WBIs are calculated in the NBO program from the same atomic hybrids that underlie the LMO construction and are therefore closely connected to the NMR parameter analyses presented below. As stated by Mayer,^[63] the sum of an atom's WBIs "corresponds very well to the chemical notion of valence". To put the WBIs of the H-bonded systems in perspective, the $WBI(O^c-H^a)$ for either one of the ethanol conformers is 0.76 and $WBI(N^c-H^a)$ is 0.79. The lower-than-1 reference values indicate the polarity of the X–H bonds. For the hydrogen-bonded systems, $WBI(X^c-H^a)$ weakens in favor of $WBI(H^a-X^b)$; the sums of $WBI(X^c-H^a)$ and $WBI(H^a-X^b)$ in the H-bonds are roughly the same as the WBI of the non-hydrogen bonded reference systems. As shown below, the differences in the bond orders go along with qualitatively and quantitatively different magnetic properties related to the protons in the H-bonds.

For the RAHB systems PD, MA and NMD, orbital interactions between H^a and O^b across the hydrogen bond are indicated by WBIs on the order of 0.1. For 3OH the $WBI(H^a...O^b)$ bond order is only half that of these resonance-stabilized systems MA. The 3OH is a system without π conjugation in the backbone. The difference in the WBIs is therefore significant, as it shows that breaking the π -conjugation results in a large relative loss of covalent character of the $H^a...O^b$ interaction and a concomitant increase of the O^c-H^a bond order. DHP, which is also not resonance stabilized, has an even smaller $H^a...O^b$ bond order than 3OH, while the O^c-H^a bond order is nearly as high as that of ethanol. The molecule NMA is unlike PD, MA and NMD in the sense that the optimized structure affords a more symmetric $O^c-H^a...O^b$ arrangement where bonding with the proton is more evenly shared among the two oxygen atoms. Not surprisingly, the $WBI(H^a...O^b)$ is much larger in this system, reaching 0.33, while the O^c-H^a bond index drops to 0.42. Due to this difference in the H-bonding, NMA is discussed separately

from other RAHB systems in the following. The anionic HSA also affords a particularly large $H^a...O^b$ bond order. We already mentioned in the introduction that the proton in this system is particularly de-shielded. The bond orders for AAD are comparable to those of MA, raising the question of how important resonance is for this system. The NH bond orders for the hydrogen bonds of the DNA base pairs, on the other hand, are more comparable to the OH bond orders of 3OH, both in magnitude and in relation to the X–H reference WBIs.

The differences in the $WBI(H^a...X^b)$ versus $WBI(H^a-X^c)$ are correlated with the differences between the distance of the proton to the respective oxygen atoms or nitrogen atoms, listed in Table 2 as D_{XHx} ($X=O, N$) which is the criterion of Limbach and co-workers mentioned in the Introduction. That is, more equal $X^c-H^a...X^b$ distances (small D_{XHx}) go along with smaller differences in the corresponding WBIs.

Isotropic proton shifts and proton shielding tensors

Isotropic NMR shielding data of the H-bonded protons for the molecules of Figure 1 are collected in Table 2. Ethanol shielding constants are provided in the footnotes of the same Table. In the following, the EtE conformer is used for further comparisons with the other molecules. Additional calculated data can be found in Tables S1, S2, and S4 in the Supporting Information for different functionals and basis sets, and a comparison of STO with GTO basis sets, demonstrating that the PBE0/TZP data discussed herein are sufficiently well converged with respect to basis set size and that the H^a shielding is not strongly dependent on the functional.

As we are concerned with rather anharmonic potential energy surfaces (PESs), ZPV corrections $\Delta\sigma_0$ to the H^a shielding constants were calculated as described in reference [58]. To first order, there are two correction terms. One arises from the effective ZPV averaged geometry of the molecule being different from the equilibrium structure, which is driven by the anharmonicity of the PES. The other one arises from the curvature of the shielding hypersurface around the equilibrium structure. The anharmonicity effect strongly dominates the ZPV corrections. The shielding including these anharmonicity corrections can also be obtained by a single-point shielding calculation at the ZPV averaged effective geometry (σ_{eff}). This has the advantage that important ZPV effects on the shielding can be included easily in the subsequent LMO analysis.

The chemical shifts in Table 2 were calculated with a reference shielding obtained by a linear fit of the calculated σ_{eff} to experimental shifts. The agreement of the effective ZPV averaged chemical shifts with available experimental data is rea-

Table 1. Wiberg bond indices^[a] (WBIs) for the hydrogen bonded systems of Figure 1.

WBI	EtE	EtS	G	3OH	PD	MA	NMD	NMA	AA ^[b]	GC	AT	HSA	DHP
X^c-H^a	0.76	0.76	0.79	0.67	0.59	0.62	0.60	0.42	0.61	0.71	0.68	0.48	0.73
$H^a...X^b$				0.07	0.12	0.10	0.12	0.33	0.10	0.06	0.09	0.28	0.02

[a] $X=N$ (for G, GC, AT) or O . WBIs^[62,63] as generated by the NBO code. [b] Intra/intermolecular WBI values for AA in the dimer. X^c , H^a , and X^b refer to the atom labels of Figure 1. For the other H-bonds in GC, $WBI(H...O)=0.07$ and $WBI(H^f...O^g)=0.04$. For the other H-bond in AT, $WBI(H...O)=0.04$.

Table 2. Isotropic nuclear magnetic shielding (σ , in ppm) and chemical shifts (δ) for the proton H^a in the hydrogen bonded systems of Figure 1. Distance measures for the hydrogen bridge are also given.^[a]

	3OH	PD	MA	NMD	NMA	AAD	GC	AT	HSA	DHP
r_{X-H}^{eq}	0.965	1.003	0.997	1.004	1.059	0.998	1.032	1.045	1.096	0.975
r_{X-H}^{eff}	2.274	1.633	1.701	1.663	1.393	1.684	1.919	1.841	1.352	1.979
r_{X-H}^{eq}	0.957	1.013	1.009	1.018	1.149	1.007	1.039	1.056	1.052	0.968
r_{X-H}^{eff}	2.357	1.642	1.680	1.634	1.246	1.671	1.916	1.825	1.293	2.022
D_{XHX}^{eq}	0.65	0.31	0.35	0.33	0.17	0.34	0.44	0.40	0.13	0.50
D_{XHX}^{eff}	0.70	0.31	0.34	0.31	0.05	0.33	0.44	0.38	0.12	0.53
S_{XHX}^{eq}	1.619	1.318	1.349	1.334	1.226	1.341	1.476	1.443	1.224	1.477
S_{XHX}^{eff}	1.657	1.328	1.345	1.326	1.198	1.339	1.478	1.440	1.172	1.495
σ_{eq}	29.90	15.96	16.91	16.29	12.23	18.15	17.84	16.26	9.93	21.87
σ_0	29.04	15.15	16.30	15.59	9.55	17.81	17.65	15.91	5.19	21.18
$\Delta\sigma_0$	-0.86	-0.81	-0.61	-0.70	-2.68	-0.34	-0.19	-0.35	-4.74	-0.69
σ_{eff}	30.40	15.93	16.26	15.45	9.33	17.68	17.58	15.83	9.29	22.26
$\Delta\sigma_{eff}$	0.50	-0.03	-0.65	-0.84	-2.90	-0.47	-0.26	-0.43	-0.64	0.39
δ_{eq}	0.31	14.25	13.30	13.92	17.98	12.06	12.37	13.95	20.28	8.34
δ_0	1.18	15.06	13.91	14.62	20.66	12.40	12.56	14.31	25.02	9.03
δ_{eff}	-0.19	14.28	13.95	14.76	20.88	12.53	12.63	14.38	20.92	7.95
$\delta(\text{exptl})$		15.4 ^[b]	13.99 ^[c]		18.9 ^[a]	13.13 ^[e]	13.02 ^[f]	13.65 ^[f]	20.07 ^[g]	9.39 ^[h]

[a] Values given for the hydrogen bridges $X^c-H^a...X^b$ according to the atom labels of Figure 1; r , D , S are distance measures in Å; σ and δ are in ppm. The r are the interatomic distances. D_{XHX} is the difference $(r_{X-H} - r_{XH})/2$ and measures the asymmetry of the distances in the H-bond bridge. S_{XHX} is the corresponding sum $(r_{X-H} + r_{XH})/2$; eq=equilibrium geometry; eff=effective geometry; 0=ZPV averaged value. PBE0/TZP shielding calculations. The chemical shifts $\delta(^1H^a)$ were computed with a reference shielding of 31.21 ppm, obtained from the intercept b when fitting $\delta(\text{exptl}) = b - \sigma_{eff}$. [b] Ref. [21]. [c] Ref. [20]. [d] Ref. [64]. [e] Ref. [26]. [f] Ref. [25]. [g] Ref. [24]. [h] Ref. [65]. For the effective geometry of EtE and EtS, the H^a isotropic shielding σ_{eff} is 33.03 and 33.33 ppm, respectively. For PD and HSA, contributions to the vibrational effects from one and four low-frequency modes, respectively, were excluded due to numerical noise.

sonable (see also Figure S1 and Table S1 in the Supporting Information). It is well known that DFT calculations of shielding differences for atoms in different bonding environments such as X-H for our samples versus C-H for TMS may afford systematic errors. Using a secondary reference with the reference nucleus in a chemically similar environment as the probe nuclei, or using a fit as done here, are established protocols to improve calculated chemical shifts.^[66,67] Application of a continuum solvation model did not significantly alter the calculated proton shielding constants in the H-bonds in test calculations (Table S3 in the Supporting Information), although this is not expected to be generally the case. Remaining differences between the calculated shifts and experimental data are attributed mainly to solvent effects^[23] beyond those furnished by a continuum model, dynamic effects beyond those furnished by the lowest-order perturbation-theoretical treatment of vibrational corrections, and "cross terms" between these effects. There is also a possibility that the partial bond breaking/bond formation in the systems with the largest proton shifts exposes approximations in the density functionals that are not as noticeable when calculating proton NMR shifts in more typical ranges. Overall, it is important to note that the large proton shielding range and the experimental trends within the molecule set are reproduced by the calculations. We therefore proceed with an analysis of the computational data for isolated systems with fixed structures, incorporating vibrational effects via use of the effective geometries.

It is evident from the isotropic shielding constants that 3OH affords an OH proton shielding that is closest to a non-H-bonded hydroxyl group. Compared with gas-phase ethanol, a de-shielding between 3–4 ppm occurs due to the H-bond in

3OH, depending on whether the effective or the equilibrium geometry is used. DHP, which is not a system where one expects resonance to play a large role, exhibits a more pronounced de-shielding and therefore makes for an interesting comparison with 3OH in the LMO analysis. Relative to 3OH the H^a shieldings in PD and MA decrease by 13 to 14 ppm. The roughly comparable decrease of the proton shielding in the series correlates nicely with systematic changes in the WBI($H^a...O^b$): none to 0.07 to 0.10 and 0.12 when going from EtE to 3OH to MA and PD. The H^a shielding constant for NMD is comparable to PD and MA, hinting as comparable effects from the backbone resonance (as shown below).

For NMA, the more equal sharing of the proton by the two oxygen atoms causes an even larger reduction in the H^a shielding, to only 12.2 ppm (eq) from the present STO basis PBE0 calculations, and 12.6 ppm as calculated in previous work^[16] with the B3LYP functional and a GTO basis. The de-shielding in HSA is similarly dramatic. AAD (H \cdots O hydrogen bonds) and the two DNA base pairs (for the N-H \cdots N hydrogen bonds) exhibit comparable proton de-shielding in roughly the same range as for the RAHB systems. Below, we analyze whether resonance plays any role in the de-shielding of the H-bonded proton in these systems.

As demonstrated by the data in Table 2, for most of the molecules in the test set the vibrational corrections $\Delta\sigma_0$ and $\Delta\sigma_{eff}$ are of the same sign and roughly of the same magnitude. The case where the vibrational corrections differ most strongly is HSA, a molecule that is susceptible to perturbations in part due to its negative charge. The $\Delta\sigma_0$ correction appears to be too large, indicating that the vibrational correction treatment at lowest order of perturbation theory is not sufficient for this

1 system. However, the magnitude of the $\Delta\sigma_{\text{eff}}$ correction is in-
2 line with some of the RAHB systems. NMA also exhibits
3 a rather large negative vibrational correction to the shielding,
4 possibly somewhat overestimated, but here $\Delta\sigma_{\text{eff}}$ and $\Delta\sigma_0$
5 are in reasonable agreement. For the systems MA, NMD, NMA,
6 AAD, AT, and HSA, the negative vibrational corrections go
7 along with a decrease of D_{XHx} by 0.01 or more when going
8 from the equilibrium to the effective geometry, meaning that
9 in the vibrationally averaged structures the H-bonds are more
10 symmetric. For a deuterated H-bond, as expected, the vibra-
11 tional corrections to the shielding and the structures are small-
12 er overall, as evidenced by the comparison for MA and NMA in
13 Table S9 in the Supporting Information. In cases where $\Delta\sigma_{\text{eff}}$
14 is positive (3OH and DHP), D_{XHx} increases. Overall, the ordering
15 of D_{XHx} from highest to lowest correlates well with the order-
16 ing of the proton shielding from highest to lowest, and with
17 the ordering of the chemical shifts from lowest to highest,
18 both for the equilibrium and for the effective structures. The
19 present calculations confirm the correlation of D_{XHx} with the
20 proton shifts noted previously by Limbach et al. ■ ■ ref? ■ ■

21 Additional information related to this correlation can be
22 gathered from Figure 2. Here, the relative energy of NMA and
23 the proton shielding are plotted for varying positions of the
24 proton within the molecular plane (B3LYP/TZP). The remainder
25 of the structure was held fixed. The contour plot of the energy
26 in the top row shows one minimum corresponding to the opti-
27 mized equilibrium structure rather than a double minimum
28 PES. Constrained optimizations were also performed to bring
29 about two minima in the two-dimensional scan but the surfa-
30 ces afforded too much numerical noise. Instead, a structure
31 corresponding to an average of the two minimum structures
32 with H^a bound to O^b and O^c, respectively, was generated in
33 order to see whether the shielding surface is sensitive to small
34 changes in the backbone structure related to the proton posi-
35 tion. Both sets of data are displayed in Figure 2. The shielding
36 surfaces compare well, and clearly show that the lowest
37 proton shielding—slightly above 9 ppm—is found if the
38 proton is located halfway between the two oxygen atoms,
39 with a shallow minimum region in the shielding surface along
40 the direction perpendicular to the O–O vector. Within this shal-
41 low minimum region (vertical in the plots), D_{OHo} is very zero
42 or close to zero. Obviously, the actual position (or position range)
43 of the proton is driven by the overall energetics of the system,
44 which may (for NMA) or may not be influenced by resonance
45 in the backbone. The analysis of the shielding and J -coupling
46 constants, discussed below, shows that resonance contribu-
47 tions are directly evident in the proton NMR parameters of sev-
48 eral of the systems studied here.

49 Polar plots of the various H^a shielding tensors, indicating the
50 sign and magnitude of the principal components (PCs) and the
51 orientation of the principal axis system (PAS), are shown in
52 Figure 3. The corresponding numerical data (PCs, and a break-
53 down into diamagnetic and paramagnetic shielding compo-
54 nents) are provided in the Supporting Information in Table S5.
55 For most systems the H^a shielding tensors are strongly aniso-
56 tropic as well as asymmetric. AAD, GC, and AT exhibit a H^a
57 shielding tensors similar to the PD, MA, and NMD molecules,

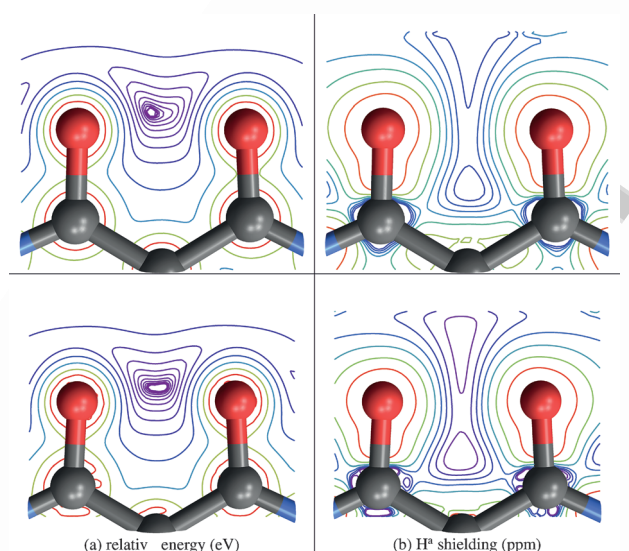


Figure 2. NMA molecule: Top row: contours for: a) the energy relative to the optimized minimum structure, and b) the corresponding isotropic NMR shielding for H^a, as a function of the position of the H^a proton in the OCCCO plane with the remaining atomic positions kept fixed. Contours at: a) 0.003×2^n eV, b) $(9 + 2n + 0.5 \times 2^n)$ ppm; with $n = 0, 1, 2, 3, \dots$ (purple to red); 1 eV corresponds to approximately 96.5 kJ mol^{-1} . Bottom row: same as top row, but with a backbone structure corresponding to an average of the two minima with the proton bound to the left and right oxygen, respectively. Minor dis-symmetries in the bottom row plots are due to numerical noise.

which goes along with similar isotropic shieldings. For NMA, two of the PCs are very small and differ in sign, leaving essentially only the one dominant component visible in the plot. HSA is qualitatively similar in terms of the tensor components and orientation. As noted already, NMA and HSA have the smallest D_{OHo} values and the largest $\text{WBI}(\text{H}^{\text{a}} \cdots \text{O}^{\text{b}})$ within the set of molecules.

From the breakdown in Table S5 in the Supporting Information, the formation of regular to strong H-bonds goes along with the appearance of small to large negative paramagnetic shielding tensor components as well as corresponding changes in the diamagnetic shielding tensor components. With the commonly adopted partitioning of the total shielding into origin-invariant paramagnetic and a diamagnetic parts,^[68] changes in the latter across a set of molecules are typical for hydrogen. For heavier elements, the diamagnetic part of the shielding tensor tends to be very similar among different compounds. The paramagnetic part of the tensor is related to field-induced paramagnetic current densities that can qualitatively be understood in terms of “orbital rotation” models.^[69] For hydrogen, we can relate the trends in the diamagnetic part of the shielding tensor to a local increase or loss of electron density. The fact that both contributions are important and have different physical origins somewhat complicates the analysis for hydrogen.

Overall, relative to EtE and guanine we find a net de-shielding in all principal components of the H^a shielding tensors of the H-bonded systems, the least for 3OH and the strongest for NMA and HSA, leading to in the observed large positive chemical shifts for the systems with strong H-bonding. The tensor

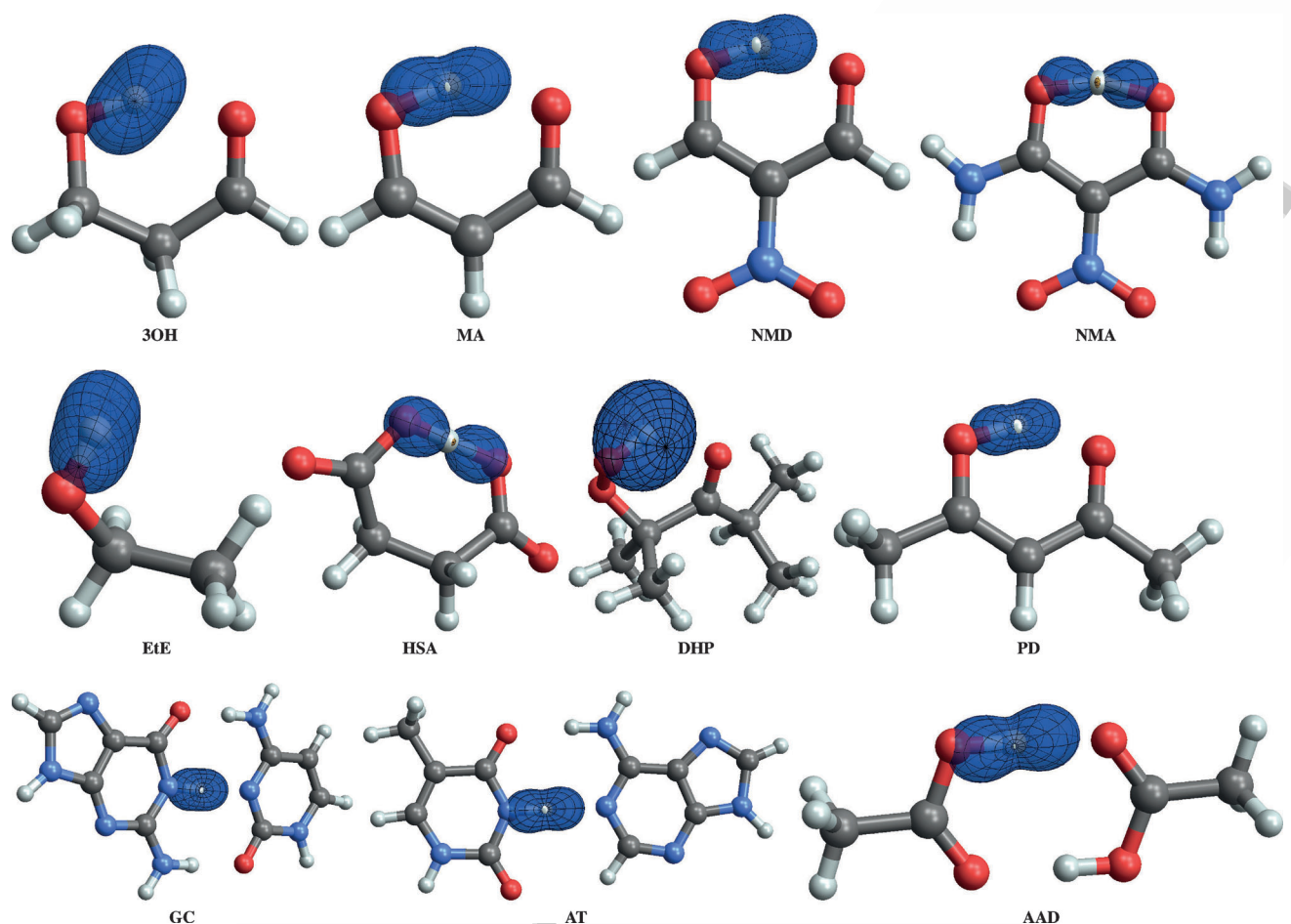


Figure 3. Polar plots of H^a proton NMR shielding tensors (shielding in the direction of the field). Molecule labels as in Figure 1. The scaling factors for the surfaces are 3OH=2.4, MA=3.5, NMD=3.5, NMA=3.5, EtE=2.0, AAD=3.5, GC=3.5, AT=4.0, HSA=4.5, PD=4.0; all in ppm pm^{-1} . Blue/darker shading indicates a positive shielding component while orange/light shading indicates negative shielding. An isotropic shielding tensor would be represented by a sphere.

component σ_{33} is typically the one pointing along the $H^a \cdots X^b$ direction and exhibiting large negative paramagnetic shielding contributions in the case of strong H-bonding. Negative paramagnetic contributions in the other two PCs add up to roughly the same magnitude as that in σ_{33} for HSA, PD, MA, and to a lesser degree for AAD. For NMA, all H^a shielding tensor components afford large paramagnetic contributions (between -11 and -13 ppm), while for GC and AT the presence of the H-bond creates paramagnetic contributions mainly in σ_{33} . The H^a shielding tensor orientation for DHP is such that σ_{33} coincides with the $H^a \cdots O^b$ direction, due to the twist in the geometry caused by the O–O–H moiety. Indeed, Table S5 in the Supporting Information reveals that it is component σ_{22} of DHP that has a -12 ppm paramagnetic contribution whereas those in σ_{11} and σ_{22} are comparatively small.

Despite the fact that the tensor character^[70,71] of nuclear magnetic shielding and J -coupling is pronounced for our samples, one may expect most measurements on hydrogen-bonded systems to be carried out in solution or with magic-angle spinning techniques for solids. For this reason, and for brevity, the present LMO analysis focuses on the isotropic shieldings and coupling constants.

Nuclear magnetic shielding analysis

We now turn to the LMO analysis of the nuclear magnetic shielding, with a focus on contributions that render the H^a shielding constants particularly small. Relative to a reference XH group, this can be indicated by less positive or more negative contributions from orbitals centered around X, and by new negative contributions from orbitals that are absent for the reference. Due to the similarity of PD to MA and of AT to GC, the analysis was not carried out for PD and AT. Selected LMOs are shown in form of isosurface plots in Figure 4, Figure 5 and Figure 6, along with labels indicating their local σ or π symmetry.

An extended set of LMO plots is provided in the Supporting Information, Figures S5 to S12. For sake of space, not all LMOs are shown. The LMOs listed in the Tables are those that produce important contributions to the analysis. Some of these are displayed graphically as representatives for a class of LMOs that are similar among the molecules, others to illustrate their delocalization or orientation for a particular molecule. A representative for the X^c-H^a σ bond LMO can be found in Figure 6. For convenience, some LMOs are labeled by coordinates

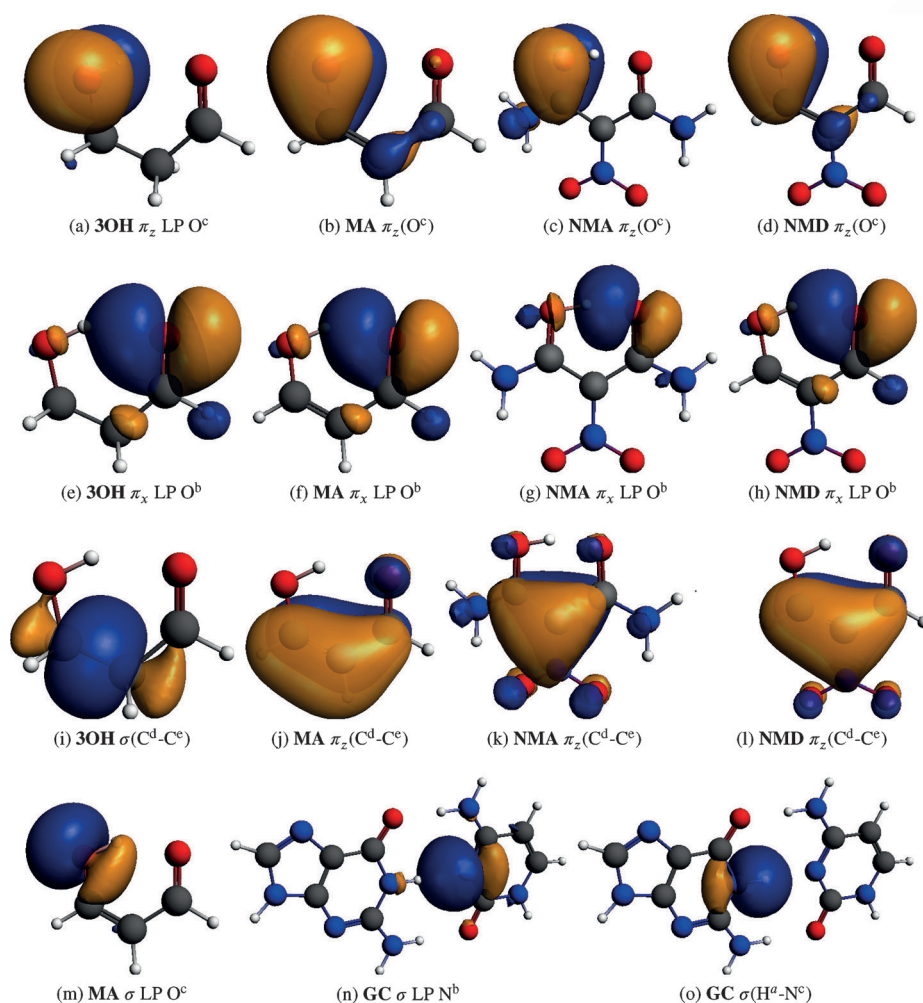


Figure 4. Selected LMOs (shown as isosurfaces, ± 0.03 a.u.) for a subset of the hydrogen-bonded systems. For atom labeling see Figure 1. $\pi_z(\text{O})$ may refer to $\pi_z(\text{C}-\text{O})$ or a π_z LP on an oxygen, or a multicenter orbital with strong oxygen π_z character.

x and/or y , indicating their direction in the $\text{X}^{\text{c}}-\text{H}^{\text{a}}\cdots\text{X}^{\text{b}}$ plane, with x roughly parallel to the $\text{H}^{\text{a}}\cdots\text{X}^{\text{b}}$ direction (pointing horizontally in the plots), and y roughly vertical. The z direction is

perpendicular to the molecular plane (i.e., perpendicular to the paper/screen). Numerical data characterizing the LMOs are provided in Table 3 and Table 4.

Intramolecular hydrogen bonds

The shielding data for H^{a} of EtE and the systems with intramolecular H-bonds are provided in Table 5, Table 6, and Table 7. The Tables also include the occupations n of the “parent NBO” of each LMO. These parent NBOs are idealized one- or two-center LP, core, or bonding orbitals related to the chemical Lewis structure.^[40] An occupation of the parent NBO of much less than two means that the corresponding LMO has significant contributions from other NBOs, indicating delocalization (in turn, a given parent NBO may or may not contribute to other LMOs). The numerical breakdown in Table 3 and Table 4 characterizing the LMO sets provides further information about delocalization. It is worthwhile reiterating that the presence of electron delocalization means that the electron orbitals determined in quantum chemical calculations cannot be localized fully to a degree such that they represent only 1-center LPs (and atomic core orbitals) and 2-center bonds.^[72] We therefore use the presence of LMO delocalization in order to assess the

Table 3. Composition of selected LMOs of EtE, 3OH, MA, NMD, and NMA. For atom labeling see Figure 1.^[a]

	EtE	3OH	MA	NMD	NMA
$\sigma(\text{O}^{\text{c}}-\text{H}^{\text{a}})$	26 H^{a} s(100)	23 H^{a} s(100)	21 H^{a} s(100)	21 H^{a} s(100)	16 H^{a} s(100)
	74 O^{c} s(24)p(76)	76 O^{c} s(22)p(78)	78 O^{c} s(24)p(75)	78 O^{c} s(24)p(75)	82 O^{c} s(22)p(78)
π_z LP O^{c} or $\pi_z(\text{O}^{\text{c}})$	98 O^{c} p(100)	97 O^{c} p(100)	88 O^{c} p(100)	86 O^{c} p(99)	84 O^{c} p(100)
			1 C^{f} p(100)	1 C^{f} p(100)	3 N p(100)
			3 C^{e} p(100)	2 C^{e} p(100)	
σ LP O^{b}		1 C^{d} p(94)d(6)	8 C^{d} p(99)d(1)	10 C^{d} p(99)(1)	12 C^{d} p(99)d(1)
π_x LP O^{b} or $\pi_x(\text{O}^{\text{c}})$		99 O^{b} s(56)p(44)	99 O^{b} s(60)p(40)	99 O^{b} s(62)p(38)	98 O^{b} s(53)p(47)
		2 H^{a} s(99)p(1)	2 H^{a} s(99)p(1)	2 H^{a} s(99)p(1)	8 H^{a} s(100)
		2 C^{f} s(3)p(93)d(4)	2 C^{f} s(4)p(91)d(5)	2 C^{f} s(4)p(91)d(5)	1 C^{f} s(3)p(92)d(4)
		93 O^{b} s(2)p(98)	93 O^{b} s(3)p(97)	93 O^{b} s(2)p(98)	87 O^{b} s(15)p(84)
		1 C^{e} s(19)p(80)	1 C^{e} s(42)p(57)d(1)		2 O^{c} s(26)p(73)
		2 H s(100)		2 H s(100)	

[a] All numbers are in %. Explanation of the notation: For MA, for the $\sigma(\text{O}^{\text{c}}-\text{H}^{\text{a}})$ orbital 78% of the orbital density is associated with basis functions centered on O^{c} , and 21% with basis functions centered on H^{a} . The composition on the O^{c} center is 75% p, 25% s, indicating that an O^{c} sp^3 hybrid is involved. $\pi_{x/z}(\text{O})$ may refer to $\pi_{x/z}(\text{C}-\text{O})$ or a $\pi_{x/z}$ LP on an oxygen, or a multicenter orbital with strong oxygen $\pi_{x/z}$ character.

Table 4. Composition of selected LMOs of AAD, GC, DHP and HSA. For atom labeling see Figure 1.^[a]

	AAD	GC	HSA	DHP
$\sigma(\text{O}^{\text{c}}/\text{N}^{\text{c}}-\text{H}^{\text{a}})$	21 H ^a s(100) 78 O ^c s(27)p(73)	25 H ^a s(100) 74 N ^c s(30)p(70)	18 H ^a s(100) 84 O ^c s(28)p(72)	25 H ^a s(100) 75 O ^c s(25)p(75)
π_z LP O ^{c}/N^{c}/\pi_z (O^c)}}	89 O ^c p(100) 3 O ^b p(100) 8 C ^a p(99)d(1)	80 N ^c p(100)	87 O ^c p(100) 4 O ^b p(100) 9 C ^d p(99)(1)	99 O ^c s(12)p(88)
σ LP O ^{b}/N^b}	98 O ^b s(59)p(41)	7 C ^d p(100) 93N ^b s(32)p(68)	97 O ^b s(48)p(52)	99 O ^b p(100)
π_x LP O ^{b}/N^b}	2 H ^a s(99)(1) 3 C ^a s(1)p(96)d(3) 92 O ^b s(4)p(96)		7 H ^a s(100) 1 C ^g s(5)p(92)d(5) 88 O ^b s(80)p(20) 2 O ^c s(35)p(65)	0.4 H ^a s(98) 3 C ^f p(96)d(4) 94 O ^b p(100) 1 C ^e s(32)p(68)

[a] All numbers are in %. See footnote of Table 3 for an explanation of the notation.

Table 5. Contribution of the LMO analysis of the isotropic H^a shielding σ (in ppm) for EtE and a subset of the H-bonded systems. For atom labeling see Figure 1. Selected LMOs are shown in Figure 4.^[a]

LMO	EtE		3OH		MA		NMD		NMA	
	<i>n</i>	σ								
$\sigma(\text{O}^{\text{c}}-\text{H}^{\text{a}})$	1.99	19.47	1.99	17.87	1.98	13.30	1.98	12.25	1.97	3.90
$\pi_z(\text{O}^{\text{c}})$	1.96	5.74	1.95	5.30	1.76	3.44	1.72	3.90	1.71	3.36
σ LP O ^c	1.98	4.34	1.98	3.42	1.97	1.27	1.97	0.92	1.96	0.02
$\sigma(\text{O}^{\text{c}}-\text{C}^{\text{d}})$	2.00	4.15	1.99	4.96	2.00	3.02			1.99	2.60
$\sigma(\text{C}^{\text{e}}-\text{H})$	1.99	0.10	1.96	-0.05	1.98	-0.13				
$\sigma(\text{C}^{\text{d}}-\text{C}^{\text{e}})$	1.99	0.02	1.99	0.13	1.99	-0.96	1.99	-0.88	1.98	-0.59
core C	2.00	-0.06								
core O ^c	2.00	-0.24	2.00	-0.35	2.00	-0.30	2.00	-0.30	2.00	-0.25
$\sigma(\text{C}^{\text{d}}-\text{H})$	1.99	-0.49	1.99	-0.57	1.99	-0.89	1.99	-0.76		
$\pi_z(\text{C}^{\text{d}}-\text{C}^{\text{e}})$			1.99		1.81	0.87	1.74	0.54	1.32	0.66
σ LP O ^b			1.98	-0.51	1.98	-1.06	1.97	-1.36	1.96	-0.51
π_x LP O ^b			1.88	-0.33	1.85	-3.43	1.84	-2.77	1.73	-3.12
$\pi_z(\text{C}^{\text{f}}-\text{O}^{\text{b}})$			1.99	0.26	1.98	1.41	1.98	1.44	1.99	3.17
$\sigma(\text{C}^{\text{f}}-\text{O}^{\text{b}})$			2.00	0.48	2.00	0.75	2.00	0.79	1.99	2.16
$\sigma(\text{C}^{\text{d}}-\text{O}^{\text{b}})$							1.99	2.93		
$\sigma(\text{C}^{\text{f}}-\text{H})$			1.99	-0.36	1.99	-0.65	1.99	-0.47		
π_z nitro-O							1.75	-0.53	1.72	-0.43
$\sigma(\text{C}^{\text{d}}-\text{N})$									1.99	-0.71
$\sigma(\text{N}-\text{H})$									1.99	0.67
$\sigma(\text{C}^{\text{f}}-\text{N})$									1.99	-0.63
$\sigma(\text{C}^{\text{e}}-\text{C}^{\text{f}})$			1.99	0.37			1.99	-0.38	1.98	-0.52
$\pi_z(\text{N}-\text{O})$							1.98	0.24	1.99	0.23
core C ^f			2.00	-0.08	2.00	-0.13	2.00	-0.09	2.00	-0.04
core O ^b			2.00	-0.04	2.00	-0.08	2.00	-0.07	2.00	-0.21
$\sigma(\text{C}^{\text{e}}-\text{N})$							1.99	0.17	1.99	0.13
π_x nitro-O									1.89	-0.30
π_z LP N									1.69	-0.26
core C ^d			2.00	-0.06	2.00	-0.08	2.00	-0.06	2.00	-0.03
core C ^e			2.00	-0.05	2.00	-0.09	2.00	-0.04	2.00	-0.02
$\sigma(\text{N}-\text{O})$							2.00	0.08	1.99	0.04
$\pi_z(\text{C}^{\text{d}}-\text{N})$									1.99	0.07
core O							2.00	-0.02	2.00	-0.03
core N							2.00	-0.01	2.00	-0.04
σ LP nitro-O							1.98	-0.06	1.98	0.02
Σ analysis		33.03		30.40		16.26		15.45		9.33
calcd		33.03		30.40		16.26		15.45		9.33

[a] Additional isosurface plots of LMOs can be found in the Supporting Information; *n* is the occupation number of the parent NBO of a given LMO. $\pi_{xz}(\text{O})$ may refer to a $\pi(\text{C}-\text{O})$ bond or a π LP on an oxygen, or a multicenter orbital with strong oxygen π character. Some of the listed contributions combine several similar LMOs; in this case the occupations are averaged and the shielding contributions added; Σ is the sum of all LMO contributions and shown to be equal to the total calculated isotropic shielding (calcd).

extent of resonance in the samples. The terms resonance and delocalization are used interchangeably in this context.

Consider, first, the H^a shielding change when going from ethanol (Et) to 3OH. The LMOs of 3OH do not indicate delocal-

ization except for the in-plane carbonyl oxygen O^b LP (π_x -LP(O^b)). One of the lobes of this LMO is seen to overlap with the H^a proton (also for the other systems with $H\cdots O$ hydrogen bonds) and therefore the parent NBO occupation of 1.88 indicates some sharing of its electron density with H^a . In Table 5, the contribution from this π_x -LP(O^b) orbital to the H^a shielding in 3OH is negative, -0.3 ppm, and augmented by another -0.5 ppm from the other O^b lone-pair, σ -LP(O^b). These negative contributions are partially counterbalanced by positive shielding from the carbonyl σ and π C=O bonds. The presence of the H-bond in 3OH is accompanied by a reduction of the $\sigma(O^c-H^a)$ bond contribution to the H^a shielding from 19.5 in Et to 17.9 ppm in 3OH, correlating with the reduction of the WBI(O^c-H^a) noted above, and reductions of the shielding contributions from the two O^c lone pairs (partially counterbalanced by an increase of the shielding attributed to the O^c-C^d σ -bond). There are other differences between EtE and 3OH as well, due to the general fact that in LMOs are not perfectly transferable between molecules. However, the main change when going from Et to 3OH is quantified by a decrease of H^a shielding from the O^c-H^a bond and the O^c LPs, along with negative contributions from the O^b in-plane LP orbitals. This finding is chemically intuitive and generates a "local" interpretation of the H-bond effect on the H^a shielding, by associating it with the σ orbitals centered on atoms within the hydrogen bond.

Next, consider the π -conjugated systems MA and NMD, versus Et and 3OH. The reduction in the shielding contribution from $\sigma(O^c-H^a)$ relative to Et is much larger for these systems than for 3OH. The shielding reduction from $\sigma(O^c-H^a)$ correlates well with the calculated WBI(O^c-H^a) discussed above. Furthermore, for MA and NMD there is evidence of a direct participation of the C=C π bond in the H^a shielding. Interestingly, this contribution is negative when the analysis is performed for the equilibrium structures of MA, NMD, and NMA (not shown) but positive for the effective geometries. Its sign is therefore less important than the fact that the contribution shows up in the H^a shielding analysis in the first place. The parent NBO occupations of $\pi_z(C^d-C^e)$ for MA and NMD are only 1.81 and 1.74, respectively, indicating a strong delocalization in the backbone π system. The corresponding LMO plots in Figure 4, which include the delocalization contributions, show a pronounced multicenter character of $\pi_z(C^d-C^e)$, involving both atoms of the carbonyl group in addition to C^f and C^g , and in the case of NMD additionally the nitro and amine groups. Delocalization toward the π backbone is also evident in the π_z LP of O^c for the π -conjugated systems, whereas the corresponding orbital in 3OH exhibits the expected 1-center character of a well-localized lone pair. The parent NBO occupations in Table 5, 1.95 for 3OH but below 1.8 for the π -conjugated systems, confirm this visual assessment. This loss of electron density from O^c toward the π backbone goes along with a significantly reduced contribution of this orbital to the H^a shielding (compare 3OH with the RAHB systems) which, however, is counterbalanced by an increased H^a shielding contribution from the O^b carbonyl group π bond $\pi_z(C^f-O^b)$.

As a result of the π conjugation and the concomitant strengthening and increased symmetrization of the H-bond,

the negative contributions from the O^b LP orbitals to the H^a shielding are much larger in MA and NMD than in 3OH. The direct involvement of the C=C bond in the H^a shielding, the simultaneous reduction of the H^a shielding contributions from $\sigma(O^c-H^a)$ and the O^b LP orbitals when going from 3OH to MA and NMD, and the trends for $\pi_z(C^f-O^b)$ constitute clear evidence of the resonance stabilization of the H-bond. As revealed by the LMO analysis, the reduction in shielding as the proton assumes a position with small(er) D_{OH^a} (c.f. Figure 2) is primarily caused by the decrease of the $\sigma(O^c-H^a)$ bond and σ LP O^c shielding contributions and an increase of the negative O^b in-plane LP contributions, that is, by the orbitals in the σ framework. At the same time, the charge flow in the π system from O^c to O^b due to resonance is reflected in the H^a shielding contributions from $\pi_z(C^f-O^b)$ and $\pi_z LP(O^c)$, with a net negative change when going from 3OH to MA, along with the appearance of a contribution from the strongly delocalized $\pi_z(C^d-C^e)$ backbone orbital.

The trends when going from 3OH to NMA are qualitatively similar but even more pronounced. The most significant feature of the LMO shielding analysis is the dramatic reduction of the $\sigma(O^c-H^a)$ bond contribution to the H^a shielding to only 4 ppm (compared to 18 ppm for 3OH). The reader is reminded that this system has a more symmetric $O^c-H^a\cdots O^b$ arrangement than the other systems. Indeed, Arnold and Oldfield^[14] alluded to an exponential onset of covalency in $H\cdots O^b$ as a H-bond becomes more symmetric. The dramatic reduction of the $\sigma(O^c-H^a)$ shielding contribution compared to the other systems indicates a similarly strong distance dependence on the O^c-H^a side due to a sudden loss of covalency at increasing distances. As demonstrated below, the J -coupling constants reveal both O^c-H^a and $H^a\cdots O^b$ covalent character for NMA, with the former being more pronounced than the latter but very significantly reduced compared to PD, MA, and NMD. These findings correlate with the WBIs from Table 1. Inspection of the last column in Table 3 gives additional insight regarding the numerical values of the WBIs for NMA compared to the other RAHB systems: The composition of the LMO $\sigma(O^c-H^a)$ for NMA has the least H^a character within the set, while the π_x LP of O^b has the largest H^a character.

Similar to NMA, the charged HSA system exhibits a comparatively large WBI($H^a\cdots O^b$), a comparatively small WBI(O^c-H^a), a small D_{OH^a} value and a very low H^a NMR shielding. Selected orbitals are displayed in Figure 5 and Figure S12 in the Supporting Information.

The H^a shielding analysis is provided in Table 6 and points to strong similarities between HSA and NMA, as well as some important differences. When the H^a shielding contributions from $\sigma(O^c-H^a)$, $\pi_z(O^c)$, $\pi_x(O^b)$, and $\pi_z(O^b)$ are added, their sum is similar for the two molecules, 6.15 ppm for HSA versus 7.31 for NMA. The $\pi_z(O^c)$ orbitals contribute almost equally in both molecules. $\pi_z(O^b)$ in HSA is a strongly delocalized 3-center orbital stretching over the carboxylate group. The NBO calculation labels it as an O^b lone pair but the NBO occupation is only 1.69 and the 3-center character is evident in the isosurface plot. $\pi_z(O^c)$ has a very similar appearance as $\pi_z O^b$. For NMA, the oxygen O^b and O^c π_z orbitals do not appear quite as symmetric

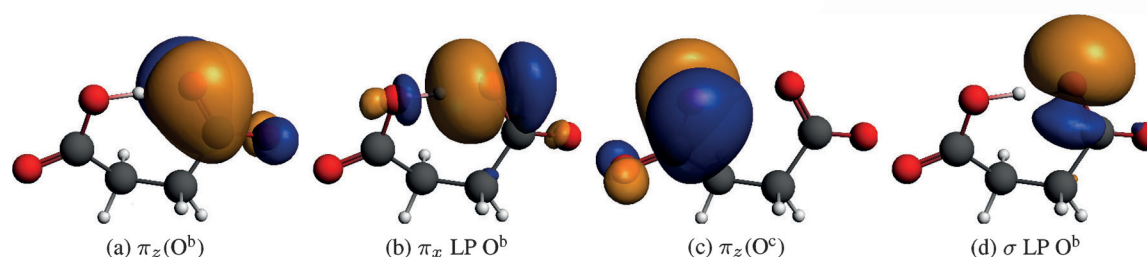


Figure 5. Selected LMOs (shown as isosurfaces, ± 0.03 a.u.) for HAS.

but rather as a LP with 3-center character on O^c and a 2-center $O-C$ π bond around O^b . In the RAHB systems, $\pi_z(O^b)$ contributes 1.5 to 3 ppm to the H^a shielding. For HSA the carboxylate $\pi_z(O^b)$ behaves similarly, 1.9 ppm. Therefore, it appears that the presence of a delocalized $\pi_z(O^b)$ orbital goes along with a positive contribution to the shielding of H^a no matter if the resonance is across the backbone or not. The carboxylate groups of HSA are overall electron rich compared to the H-bond acceptor moieties of the other molecules, which increases the negative effect from π_x LP O^b (-5 ppm) relative to the RAHB systems (-3 ppm). $\sigma(O^c-H^a)$ gives a larger contribution in HSA than NMA, and less than for MA, PD. This trend intuitively follows the corresponding WBIs. Overall, the H^a shielding in HSA is low for the following main reasons: 1) compared to the RAHB systems some positive contributions associated with the backbone π resonance are missing, 2) the negative charge causes the π_x LP O^b to be a more effective electron donor and renders its negative H^a shielding contribution particularly large, 3) the O^c-H^a bond order is almost as low as that for NMA and much lower than for MA and PD, causing a comparatively small H^a shielding contribution from $\sigma(O^c-H^a)$.

The shielding analysis for DHP is provided in Table 7. None of the parent NBO occupations indicate strong resonance in

this system, as expected. This molecule affords a hydrogen bond that is formally similar to 3OH. The parent NBO occupations of the π_x LP O^b for both systems is 1.88 and both orbitals give small negative contributions to the respective H^a shielding constants. It is further reassuring that the $\sigma(O^c-H^a)$ contributions to the H^a shielding are very similar for both systems, which goes along with a very similar percentage of electron density associated with H^a in these orbitals (see Tables 3 and 4). In 3OH, there are three other large positive H^a shielding contributions, 8.7 ppm combined from the two O^c lone pairs and 5.0 ppm from the O^c-C^d σ bond, adding up to 13.7 ppm. For DHP, the O^c-O^d σ bond contributes similarly to the H^a shielding as $\sigma(O^c-C^d)$ in 3OH, but the combined O^c LP contributions are reduced to only 2.7 ppm and there is -1.4 ppm from one of the O^d lone pairs. The main difference between 3OH and DHP can therefore be attributed to a loss of H^a shielding from the O^c lone pairs caused by a negative inductive effect from the second oxygen. This finding is chemically intuitive.

Table 6. LMO analysis of the isotropic H^a shielding for HSA. Selected LMOs are shown in Figure 5 and in Figure S12 in the Supporting Information.^[a]

LMO	<i>n</i>	σ	LMO	<i>n</i>	σ
$\sigma(O^c-H^a)$	1.98	7.35	$\sigma(C^e-C^d)$	1.99	-0.24
π_x LP O^b	1.77	-5.35	core O^b	2.00	-0.18
$\sigma(O^c-C^d)$	2.00	3.49	$\sigma(C^e-H)$	1.98	-0.14
$\pi_z(O^c)$	1.75	3.13	core C^e	2.00	-0.09
$\sigma(C^g-O^b)$	2.00	2.21	$\sigma(C^f-H)$	1.98	-0.08
$\pi_z(O^b)$	1.69	1.92	core C^f	2.00	-0.08
σ LP O^b	1.96	-0.85	core O	2.00	-0.04
$\sigma(C^d-O)$	2.00	-0.78	core C^g	2.00	-0.03
$\sigma(C^g-O)$	2.00	-0.63	$\sigma(C^f-C^g)$	1.99	-0.02
π_y LP O	1.88	-0.62	core C^d	2.00	-0.01
σ LP O	1.98	0.50	$\pi_z(O)$	1.94	0.39
core O^c	2.00	-0.33	Σ analysis		9.29
σ LP O^c	1.96	0.28	calcd		9.29
$\sigma(C^g-C^e)$	1.98	0.26			

[a] $\pi_z(O)$ may refer to $\pi_z(C-O)$ or a π_z LP on O , or a multicenter orbital with strong oxygen π_z character. Some of the listed contributions combine several similar LMOs; in this case the occupations are averaged and the shielding contributions added. Σ is the sum of all LMO contributions and shown to be equal to the total calculated isotropic shielding (calcd).

Table 7. LMO analysis of the isotropic H^a shielding for DHP. Selected LMOs are shown in Figure S9 in the Supporting Information.^[a]

LMO	<i>n</i>	σ	LMO	<i>n</i>	σ
$\sigma(O^c-H^a)$	1.99	17.92	core O^c	2.00	-0.17
$\sigma(O^c-O^d)$	1.99	3.34	core C	2.00	-0.17
σ LP O^c	1.99	2.39	$\sigma(C^e-C)$	1.96	-0.17
π_z LP O^d	1.95	-1.43	$\sigma(C^e-C^f)$	1.98	-0.17
$\sigma(C^e-O^d)$	1.99	0.74	$\sigma(C-H)$	1.99	0.10
$\pi_z(C^f-O^b)$	1.99	0.65	$\sigma(C^f-O^b)$	2.00	0.06
π_x LP O^b	1.88	-0.64	core O^d	2.00	-0.05
σ LP O^b	1.98	-0.54	core C^f	2.00	-0.04
$\sigma(C^f-C)$	1.98	-0.41	core C^e	2.00	-0.01
$\sigma(C-C)$	1.97	0.32	core O^b	2.00	0.00
π_z LP O^c	1.98	0.30	Σ analysis		22.26
σ LP O^d	1.98	0.24	calcd		22.26

[a] Σ is the sum of all LMO contributions and shown to be equal to the total calculated isotropic shielding (calcd).

Intermolecular hydrogen bonds

For another application of the NMR shielding analysis, we consider the acetic acid dimer (AAD) as a representative for strong intermolecular $O\cdots H$ hydrogen bonds. As mentioned in the Introduction, carboxylic acid dimers may also afford very strongly de-shielded H-bonded protons; AAD has been assigned a proton chemical shift of over 13 ppm experimentally

Table 8. LMO analysis of the isotropic H^a shielding for the acetic acid dimer. Selected LMOs are shown in Figure 6.

(lr)3-5 LMO	<i>n</i>	same ^[a]	ppm other ^[a]	total
$\sigma(\text{O}^{\text{c}}-\text{H}^{\text{a}})$	1.98	13.34	-0.47	12.86
$\sigma(\text{O}^{\text{c}}-\text{C}^{\text{d}})$	2.00	4.74	0.24	4.98
π_x LP O ^b	1.85	-1.59	-1.72	-3.31
π_z LP O ^c	1.78	2.89	-0.12	2.77
$\pi_z(\text{C}^{\text{d}}-\text{O}^{\text{b}})$	1.99	0.92	1.20	2.12
σ LP O ^b	1.96	-0.11	-1.92	-2.03
$\sigma(\text{C}^{\text{d}}-\text{C})$	1.99	-0.66	-0.36	-1.01
$\sigma(\text{C}^{\text{d}}-\text{O}^{\text{b}})$	2.00	-0.17	1.11	0.94
σ LP O ^c	1.97	0.87	0.05	0.92
core O ^c	2.00	-0.35	-0.05	-0.40
$\sigma(\text{C}-\text{H})$	1.98	0.14	0.09	0.23
core C ^d	2.00	-0.07	-0.09	-0.15
core C	2.00	-0.07	-0.05	-0.13
core O ^b	2.00	-0.07	-0.03	-0.11
Σ analysis		19.81	-2.13	17.68
calcd		19.81	-2.13	17.68

[a] H^a is the OH proton of the monomer on the left in Figure 6. See Figure 1 for atom labels. The breakdown of the shielding is performed in terms of the LMOs centered in the same monomer (column "same" is for the left monomer) and for equivalent LMOs centered in the other monomer (column "other" is for the monomer on the right in Figure 6). The full set of equivalent LMOs is shown in Figure S10 in the Supporting Information. The unlabeled C is the methyl carbon. Σ is the sum of all LMO contributions and shown to be equal to the total calculated isotropic shielding (calcd).

(Table 2), similar to MA. The H^a proton shielding analysis for AAD is provided in Table 8.

Selected LMOs are displayed in Figure 6. Since the dimer has equivalent sets of LMOs in each of the monomer units, the analysis is divided up into contributions from pairs of such LMOs, one in the same monomer unit as the H-bonded proton (shown on the left in the Figures), and one in the other unit (the monomer on the right). The atom labeling was chosen to be compatible with the other systems as best as possible, that is, H^a and O^c are the hydrogen and oxygen of the hydroxyl group, and O^b is the oxygen hydrogen-bonding with H^a. C^d is the COOH carbon.

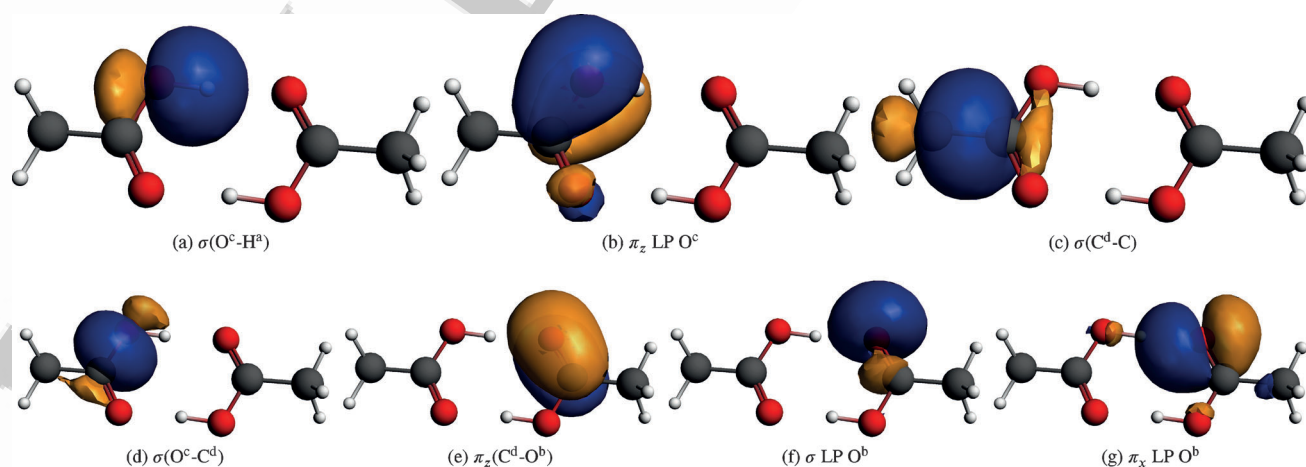


Figure 6. Selected LMOs for the acetic acid dimer (isosurfaces, ± 0.03 a.u.). See also Figure S10 in the Supporting Information.

The calculation gives a H^a shielding of 17.7 ppm for AAD, only 1.7 ppm higher than for MA. Experimentally, the trend is the same, resulting in a slightly lower proton chemical shift for AAD than MA. The contribution from $\sigma(\text{O}^{\text{c}}-\text{H}^{\text{a}})$ in the AA dimer is about 13 ppm, as small as that of MA and much below the corresponding contributions in 3OH and ethanol. The H^a shielding contribution from the same-unit $\sigma(\text{O}^{\text{c}}-\text{H}^{\text{a}})$ bond correlates well with the WBI for this atom pair: at 0.61 it is very comparable to those for MA and NMD, and significantly below those of 3OH and ethanol (Table 1). The WBI(H^a...O^b) across the H-bonds are 0.10 and also very similar to those of MA and NMD and significantly larger than for 3OH. It is further noted that the $\sigma(\text{O}^{\text{c}}-\text{H}^{\text{a}})$ bond in the *other* monomer unit contributes -0.5 ppm to the H^a shielding, which is testament to the fact that the other H-bond involves the C=O oxygen in the same unit as H^a and is therefore electronically coupled to the left monomer unit. This and many other LMO contributions reveal that there is electronic coupling between π and σ orbitals, respectively, centered in different monomer units, with quantifiable effects on the H^a shielding.

Similar to the previously discussed systems, the LP contributions from O^b of the other monomer unit are negative and sizable. This is one of the direct influences of the H-bond. The combined negative numerical value for the O^b LPs of the other unit is comparable to those of MA, and NMD, if slightly smaller in magnitude. This is accompanied by an additional negative contribution from the equivalent orbitals in the same monomer unit. The isosurface plot of the π_x LP O^b LMO reveals that the orbital has density on H^a and O^c across the hydrogen bond as well as on O^c within the same monomer unit.

The π resonance in the AA dimer is evident, for instance, from the low occupation of the parent NBO of the O^c π_z "lone pair" (1.78). Inspection of the LMO in Figure 6 shows that the orbital has a pronounced 3-center character (covering the COO unit), with O^c-C^d π bonding and some C^d-O^b π -antibonding character. The extent of delocalization of this LMO is not unlike those in the resonance-stabilized systems as well as in HSA. However, of the three centers involved, one is the C=O oxygen that H-bonds to another AA monomer. With the exception of DHP, the "same unit" π_z LP O^c shielding contribution is by far

the smallest among the systems discussed so far, and there is even a small negative contribution from the equivalent LP in the other monomer.

To summarize the AAD case, the large de-shielding of the H^a proton in the dimer has definitely a resonance component, as evidenced by the peculiar π_z LP O^c contributions. Further, the NMR analysis shows evidence of electronic coupling among σ and π orbitals centered in different monomer units. There is another factor at play here, however. The strength of the hydrogen bond places the proton at a position with comparatively small D_{OHO} , and then the loss of shielding contributions from σ orbitals (in-plane) around the proton can be considered the main driver for the low proton shielding. For AAD, the D_{OHO} value of 0.44 Å is not as low as for MA and NMA but much smaller than for 3OH, due to the combined strength of two hydrogen bonds that hold the system together. As far as the σ orbital framework is concerned, the reduction in the combined H^a shielding contributions is similar in magnitude to the RAHB systems. The same-unit π resonance in AAD, via π_z LP O^c has a stronger effect on the H^a shielding than found for the RAHB systems, resulting in a H^a shielding that is almost as low for AAD as it is for MA.

The shielding analysis for the N^c–H^a...N^b hydrogen bonded proton in the GC base pair is provided in Table 9. The calculated shielding and the calculated and experimental chemical shifts are very similar to AAD. The WBIs indicate that the proton is less shared between the heteroatoms in GC than in AAD. The D_{NHN} value is smaller than for AAD but it cannot be compared directly with D_{OHO} due to the different radii of the heteroatoms. Likewise, the H^a shielding contributions from O–H and O–N bonding orbitals are not directly comparable. However, the magnitudes and sign patterns for the orbitals centered on the H and N atoms constituting the hydrogen bond follow the same pattern as for O...H hydrogen bonds. We find a positive large contribution to the H^a shielding from $\sigma(\text{N}^c\text{--H}^a)$, a positive contribution from π_z LP N^c, and a negative contribution from one of the lone pairs of the carbonyl oxygen in the guanine moiety, indicating that another hydrogen bond is interfering with the H^a shielding.

As a reference for GC, an analysis for the H^a shielding of isolated guanine (G) is also provided in Table 9. The total effect of the N–H...N hydrogen bond on the H^a shielding is roughly –7 ppm and therefore considerably smaller overall than the effects of the O–H...O bonds on the H^a shielding in AAD. The magnitude of the de-shielding again correlates with the H^a...X^b WBI. For GC, one obtains a shielding reduction by almost 7 ppm from the presence of the H-bond by *only* adding the contributions from $\sigma(\text{N}^c\text{--H}^a)$ (GC vs. G) as well as σ LP N^b and a delocalized π_z LP N^b (GC only, with the former being negative and the latter being positive). Therefore, this creates a local interpretation of the effects of the H-bond on the H^a shielding that only involves orbitals centered on the three atoms forming the H-bond. There is an electronic coupling of the orbitals associated with the H-bond present with both the σ and π bonding frameworks, as evidenced by the many other contributions to the H^a shielding, which is to be expected in systems

Table 9. LMO analysis of the isotropic H^a shielding for the GC base pair and guanine (G).^[a]

LMO	GC		G	
	n	σ	n	σ
$\sigma(\text{H}^a\text{--N}^c)$	1.98	18.58	1.99	23.25
σ LP N ^b	1.87	–3.58	–	–
π_z LP O	1.85	–2.64	1.84	0.34
π_z LP N ^c	1.62	2.23	1.65	2.27
$\sigma(\text{C--N})$	1.99	1.97	1.98	0.01
$\sigma(\text{C--N}^c)$	1.99	1.82	1.99	–0.02
$\sigma(\text{C--N}^b)$	1.98	1.36	–	–
$\sigma(\text{C--O})$	1.99	1.24	1.99	–0.87
$\pi_z(\text{C--N}^b)$	1.78	1.06	–	–
$\sigma(\text{N--H})$	1.99	–0.97	1.99	–0.01
$\pi_z(\text{C--O})$	1.99	0.96	1.99	0.33
π_z LP N	1.66	–0.92	1.60	–0.13
core C	2.00	–0.87	2.00	0.02
σ LP N	1.91	–0.73	1.91	–0.39
σ LP O	1.97	–0.55	1.98	0.34
core N	2.00	–0.36	2.00	–0.09
$\pi_z(\text{C--C})$	1.76	0.34	1.69	0.16
core N ^c	2.00	–0.23	2.00	0.56
$\sigma(\text{C--H})$	1.98	–0.20	1.98	–0.02
core N ^b	2.00	–0.19	–	–
core O	2.00	–0.18	2.00	–0.01
$\sigma(\text{C--C})$	1.98	–0.17	1.98	–0.41
$\pi_z(\text{C--N})$	1.85	–0.14	1.89	0.07
π_z LP N ^c	–	–	1.81	0.52
$\pi_z(\text{C}^d\text{--N})$	–	–	1.84	0.04
$\sigma(\text{C}^d\text{--N})$	–	–	1.98	–0.53
$\sigma(\text{C}^d\text{--N}^c)$	–	–	1.99	–0.36
$\sigma(\text{C}^d\text{--N}^b)$	–	–	1.99	–0.67
$\sigma(\text{N}^e\text{--H})$	–	–	1.99	0.17
$\sigma(\text{N}^e\text{--H}^f)$	–	–	1.99	–0.19
Σ analysis	–	17.58	–	24.40
calcd	–	17.58	–	24.40

[a] Σ is the sum of all LMO contributions and shown to be equal to the total calculated isotropic shielding (calcd).

with extended delocalized electronic structures. However, since there is only a small net effect on the H^a shielding from these orbitals the analysis can be interpreted in a way that points to a much smaller role of electron delocalization for the H^a shielding in GC compared to several of the other systems analyzed in this study, including the intermolecular H-bond of AAD.

Fonseca Guerra et al.^[73] have previously addressed the role of resonance in the energies of DNA base pair hydrogen bonds, in particular whether there is a resonance stabilization. With the help of bond-energy decompositions it was shown that orbital interactions in the σ framework and electrostatic interactions determine the stability, while the contributions from the π system are combined an order of magnitude smaller. This analysis has recently been reaffirmed in references [74–76]. Our NMR-based interpretation of the GC N–H...N H-bond as “local” in the sense as described above is therefore entirely consistent with the energetic analysis from reference [73].

Analysis of indirect nuclear spin–spin coupling constants

Additional information about the different hydrogen bonds among our samples can be obtained from the indirect, elec-

tron-mediated, nuclear spin-spin coupling constants (J -couplings). ^1H - ^{17}O and ^1H - ^{15}N J -coupling constants, and reduced coupling constants K that are independent of the signs and magnitudes of the nuclear magnetic moments, have been calculated for the $\text{X}^{\text{c}}-\text{H}^{\text{a}}$ and $\text{H}^{\text{a}}\cdots\text{X}^{\text{b}}$ atom pairs ($\text{X}=\text{N}, \text{O}$). We wanted to learn how the spin-spin couplings vary with respect to the particular hydrogen bond transmitting the coupling. The spin-spin couplings were analyzed in terms of the same LMOs used for the shielding analysis. A breakdown in terms of the familiar spin-dipolar and "Fermi contact" spin mechanisms (SD, FC), the paramagnetic spin-orbital mechanism (PSO), and the diamagnetic spin-orbital term (DSO) is provided. The reduced couplings are collected in Table 10 and Table 11; corresponding J -coupling values can be found in Table S7 in the Supporting Information.

Table 10. Calculated reduced^[a] coupling constants K in units of $10^{19} \text{T}^2 \text{J}^{-1}$.

	DSO	PSO	FC	SD	Total
$K(\text{O}^{\text{c}}-\text{H}^{\text{a}})$ or $K(\text{N}^{\text{c}}-\text{H}^{\text{a}})$					
3 OH	0.24	3.47	40.68	-0.21	44.18
PD	0.30	2.56	54.94	-0.02	57.78
MA	0.28	2.75	56.30	0.00	59.33
NMD	0.30	2.31	54.66	0.07	57.34
NMA	0.47	-0.17	26.98	-0.03	27.26
AAD	0.33	2.92	61.33	-0.12	64.46
GC	0.50	0.52	89.32	-0.11	90.22
G	0.41	1.28	88.54	-0.20	90.03
AT	0.49	0.33	89.42	-0.11	90.13
HSA	0.48	0.49	45.76	0.00	46.72
DHP	0.25	-0.12	47.61	-0.06	47.69
$K(\text{H}^{\text{a}}\cdots\text{O}^{\text{b}})$ or $K(\text{H}^{\text{a}}\cdots\text{N}^{\text{b}})$					
3 OH	0.36	-0.64	-6.14	0.44	-5.99
PD	0.43	-1.49	-5.29	0.58	-5.77
MA	0.40	-1.58	-4.42	0.11	-5.50
NMD	0.42	-1.56	-4.25	0.20	-5.19
NMA	0.51	-0.88	11.76	0.09	11.48
AAD	0.49	-0.81	-4.73	0.34	-4.71
GC	0.50	-0.51	-2.60	-0.27	-2.88
AT	0.50	-0.59	-2.25	-0.31	-2.64
HSA	0.59	-1.14	5.01	0.24	4.70
DHP	0.36	-0.48	-2.45	0.20	-2.38

[a] Refer to Table S7 in the Supporting Information for the isotropic J -coupling values for these systems. Calculations with the effective geometries. The numerical conversion to $J(\text{H}-\text{O})$ in Hz is $-1.629 \times K(\text{H}-\text{O})$ and for $J(\text{H}-\text{N})$ it is $0.868 \times K(\text{H}-\text{N})$.

All $K(\text{X}^{\text{c}}-\text{H}^{\text{a}})$ are positive. For covalent bonds, reduced one-bond coupling constants K are typically positive,^[77,78] and typically dominated by the FC mechanism. The $K(\text{X}^{\text{c}}-\text{H}^{\text{a}})$ are no exception and therefore testify to the covalent character of these bonds. The FC mechanism, in particular, is sensitive to interatomic distances, the s character of the atomic hybrids involved in the bond, and how easily the nuclear spin magnetic moment can induce a spin density in the electronic system. The $\text{O}-\text{H}$ J - and K -couplings have opposite signs due to the negative magneto-gyric ratio of ^{17}O . Del Bene et al.^[79] have recently determined theoretical J -coupling constants for the $\text{O}-$

H bonds in methanol and hydroxyl, respectively, at the second-order polarization propagator level, which translate to K couplings of 49.1 and 40.3 in units of $10^{19} \text{T}^2 \text{J}^{-1}$. K values quoted the text below are understood to be in the same SI units. Our 3OH and DHP values for the $\text{O}^{\text{c}}-\text{H}^{\text{a}}$ pair of nuclei are in the same range.

The larger K -couplings for AAD and for the $\text{N}^{\text{c}}-\text{H}^{\text{a}}$ bonds of the DNA bases can be attributed to the increased s character of the corresponding σ -bonding LMOs at the nitrogen atoms (Tables 3 and 4). Interestingly, in the LMO analysis the main difference between the $\text{N}^{\text{c}}-\text{H}^{\text{a}}$ and $\text{O}^{\text{c}}-\text{H}^{\text{a}}$ couplings is not in the contribution from the $\sigma(\text{X}^{\text{c}}-\text{H}^{\text{a}})$ orbital but in the presence of a sizable negative contribution from the $\sigma \text{O}^{\text{c}}$ LP. It is negative because the s character of this orbital reduces the $s-\sigma$ covalent character available for the $\text{O}^{\text{c}}-\text{H}^{\text{a}}$ bond. In the nitrogen H-bonds, corresponding orbitals on N^{c} with significant s character are not present. The LMO analysis for the $K(\text{N}^{\text{c}}-\text{H}^{\text{a}})$ reinforces the local interpretation derived from the shielding analysis.

The similarity of the H^{a} shielding between the AA dimer and MA and NMD, respectively, is paralleled by a similarity of the K -couplings for the $\text{O}^{\text{c}}-\text{H}^{\text{a}}$ pair of nuclei, in terms of sign, magnitude, and relative weight of the different mechanisms (also for $K(\text{H}^{\text{a}}\cdots\text{O}^{\text{b}})$). Overall, the dominant LMO contributions in the K -coupling analysis implicate the same orbitals that are responsible for the trends in the H^{a} NMR shielding.

The coupling constants $K(\text{H}^{\text{a}}\cdots\text{X}^{\text{b}})$ across the H-bonds are also dominated by the FC mechanism. However, in relative terms the PSO mechanism is very important for the π -conjugated RAHB systems with negative K where this mechanism can reach up to about 1/3 of the magnitude of the FC terms, and for HSA. The fact that the FC and PSO mechanisms are both important for $K(\text{H}^{\text{a}}\cdots\text{O}^{\text{b}})$ testifies to the fact that concerted σ/π interactions are responsible for the stabilization of the H-bond and the strong de-shielding of the H^{a} protons in these systems.

The most striking trends are found for NMA and HSA compared to the remainder of the molecule set. For instance, $K(\text{O}^{\text{c}}-\text{H}^{\text{a}})$ is very much smaller for NMA than for the other systems, which correlates with the WBI. Table 11 collects contributions from different LMOs to the reduced $K(\text{O}^{\text{c}}-\text{H}^{\text{a}})$ coupling. The trend for NMA relative to the other compounds is consistent with a significant weakening of $\text{O}^{\text{c}}-\text{H}^{\text{a}}$ covalency and a simultaneous formation of a $\text{H}^{\text{a}}\cdots\text{O}^{\text{b}}$ covalent interaction. Each LMO contribution to $K(\text{O}^{\text{c}}-\text{H}^{\text{a}})$ of NMA is only roughly half of the equivalent contribution in the MA and NMD systems. For HSA, on the other hand, the $K(\text{O}^{\text{c}}-\text{H}^{\text{a}})$ coupling is not particularly small, which supports the aforementioned notion of a sudden loss of $\text{O}^{\text{c}}-\text{H}^{\text{a}}$ covalency as D_{OH_0} decreases.

The corresponding onset of $\text{H}^{\text{a}}\cdots\text{O}^{\text{b}}$ covalency is indicated, rather dramatically, by the fact that the only positive $K(\text{H}^{\text{a}}\cdots\text{O}^{\text{b}})$ couplings are found for HSA and NMA. NMA and HSA also give sizable positive contributions from the O^{b} core orbitals to $K(\text{H}^{\text{a}}\cdots\text{O}^{\text{b}})$; the positive sign is consistent with the presence of covalent bonds^[78] and match the positive signs of the O^{c} core contributions to $K(\text{O}^{\text{c}}-\text{H}^{\text{a}})$. The larger $\text{H}^{\text{a}}\cdots\text{O}^{\text{b}}$ K -coupling for NMA correlates with the larger $\text{H}^{\text{a}}\cdots\text{O}^{\text{b}}$ WBI for this system. There is also a sizable negative contribution from $\sigma \text{LP O}^{\text{a}}$

Table 11. LMO contributions^[a] to the isotropic reduced *K*-coupling ($10^{19} \text{ T}^2 \text{ J}^{-1}$).

	3OH	MA	NMD	NMA	AAD	GC	HSA	DHP
<i>K</i> (O ^c –H ^a) or <i>K</i> (N ^c –H ^a)								
σ LP O ^c	–47.03	–33.71	–32.35	–16.19	–33.82		–21.14	–49.77
σ (O ^c –C ^d)		–5.22		–2.90	–6.63		–4.81	
σ (X ^c –H ^a)	68.83	66.32	64.51	36.82	71.02	61.43	52.94	81.95
core O ^c /N ^c	23.82	32.05	31.42	17.84	34.44	44.36	27.91	26.30
π_z LP O ^c /N ^c	2.57	2.87	2.65	1.20	2.84	1.05	1.91	–11.78
π_x LP O ^b		–1.79	–2.37	–9.40			–8.51	
σ (C ^d –H)	–1.35	–2.11	–2.13					
π_z (O ^c –C ^d)	–2.64							
σ LP N						–1.24		
σ (C–N)						–6.66		
σ (C–N ^c)						–7.12		
σ (C ^d –C)					–1.95			
σ (C ^d –O ^b)			–5.25					
π_z LP O ^b					–1.56			
π_y LP O							–1.67	
σ (O ^c –O ^d)								1.44
Σ analysis	44.20	58.41	56.49	27.38	64.35	91.83	46.63	48.13
calcd	44.18	59.33	57.34	27.26	64.46	90.22	46.72	47.69
<i>K</i> (H ^a ...O ^b) or <i>K</i> (H ^a ...N ^b)								
σ (O ^c –H ^a /N ^c)	–2.43	–1.99	–2.34	–6.44	–2.25	–1.26	–5.83	
σ LP O ^b	–1.91	–1.30	–1.38	–8.84	–1.79		–6.21	–1.02
core O ^b	–1.14			10.26			6.89	
π_x LP O ^b		–1.04		17.75			12.08	
σ (C ^f –O ^b)				–1.74				
σ (C ^g –O ^b)							–1.90	
Σ analysis	–5.48	–4.33	–3.72	10.99	–4.04	–1.26	5.03	–1.02
calcd	–5.99	–5.50	–5.19	11.48	–4.71	–2.88	4.70	–2.38

[a] Small contributions were omitted to avoid clutter. Σ is the sum of all listed LMO contributions and shown to be close to the total calculated *K*-coupling (calcd).

(much smaller for the other molecules). It is nearly as large for HSA as it is for NMA, further underlining that there are similarities between the systems as far as the H-bonds are concerned. Positive contributions from π_x LP O^b and sizable negative contributions from the σ (O^c–H^a) bond to the H^a...O^b coupling must be interpreted as an on-set of 3-center bonding between O^c, H^a, and O^b for these geometrically more symmetric H-bonds (small D_{OH_2}).

In an analysis of a completely symmetric H-bond, one would expect the role of π_x LP O^b and σ (O^c–H^a) to become equivalent in some sense. One would further expect a σ -bonding LMO to contribute positively to the *K*-coupling of H^a with the oxygen on which the LMO is mainly centered, and negatively to the coupling of H^a with the other oxygen. An LMO analysis for a symmetrized structure of NMA indeed showed this behavior, with the usual caveat of a 3-center-4-electron bond being represented in the NBO framework as one of two possible equivalent unsymmetric resonance structures.^[17] In Table 11, the sign patterns expected for the onset of 3-center bonding are also observed for the effective structures of NMA and HSA in the sense that π_x LP O^b has large positive contributions to *K*(H^a...O^b) and sizable negative contributions to *K*(O^c–H^a), while for σ (O^c–H^a) the trend is opposite. Obviously, due to the fact that the H-bonds in these systems are not perfectly symmetric, the various contributions do not appear as mirror images. But the analysis of the coupling constants shows very clearly that

NMA and HSA have crossed a threshold where the LMOs around both oxygen atoms contribute *qualitatively* in a similar way and both oxygen atoms have covalent interactions with H^a in the H-bond.

Summary and Conclusion

The chemical shift and the indirect *J*-coupling, both routinely observed in NMR spectroscopy, are sensitive indicators of covalency in H-bonds and of the symmetry of an H-bonding environment. For the present study we have investigated these NMR spectroscopic parameters for intra- and intermolecular H-bonded protons with the help of quantum chemical calculations. The NMR parameters were analyzed in detail in terms of localized molecular orbitals (LMOs) representing chemist's bonds and lone pairs. The LMOs may exhibit varying degrees of delocalization, depending on the degree of resonance in a system. The ease, or lack thereof, by which an LMO responds to the perturbation from the spectrometer's magnetic field or from the magnetic fields generated by nuclear spin magnetic moments, is also incorporated in the analysis.

A consistent finding from the analysis is the correlation of calculated X^c–H^a Wiberg bond indices (WBIs, X=O, N) both with the H^a shielding contribution from σ (X^c–H^a) and with the size of the reduced *K*(X^c–H^a) nuclear spin–spin coupling. Furthermore, the H^a...O^b bond order across the hydrogen bond

correlates well with the H^a shielding contribution from the O^b lone-pair orbital pointing along the $H^a \cdots X^b$ axis. For most systems $K(H^a \cdots X^b)$ is negative. However, orbital–overlap interactions must be dominant factors, as evident by the direct contributions of the O^b centered LMOs. For instance, the FC mechanism decays exponentially at longer ranges^[80] and requires involvement of orbitals that have contributions on both atoms^[78] in order for the FC mechanisms in $K(H^a \cdots X^b)$ to be significant. The negative sign is reminiscent of the negative signs often found for “through space” couplings,^[81] and therefore we interpret it as driven by noncovalent interactions involving some overlap. The $K(H^a \cdots X^b)$ nuclear spin–spin coupling changes sign when going from traditional H-bonds with relatively large D_{HX} to more symmetric cases with small D_{HX} (the latter being represented by NMA and HSA molecules among our samples), with a positive sign signaling a covalent character of the $H^a \cdots X^b$ interaction and the on-set of $O^c \cdots H^a \cdots O^b$ 3-center σ bonding. A “shielding” map derived for the NMA molecule from quantum chemical calculations confirms that the H^a shielding is the lowest for the most symmetric arrangements, in agreement with the previously determined correlation of low D_{HX} with low H^a shielding by Limbach et al. ■ ■ ref? ■ ■ We remind the reader that low shielding translates into a large chemical shift.

The main characteristic of the shielding of H^a as well as the spin–spin couplings to the heteroatoms in the hydrogen bond arises from two blocks of LMOs: orbitals centered fully or partially on X^c , and LMOs centered fully or partially on the X^b atom. These orbitals generate a local interpretation of the H^a shielding. A major driver is the contribution from $\sigma(X^c \cdots H^a)$ which decreases strongly with decreasing $\text{WBI}(X^c \cdots H^a)$ /increasing $r(X^c \cdots H^a)$. The lone pairs of X^b in the σ framework generally cause de-shielding of H^a while π orbitals centered on X^b afford positive H^a shielding contributions. It is conceivable that substituents that modulate the electron density share of X^b of these orbitals would modulate the H^a shielding accordingly, as long as D_{HX} is not affected. Other sets of orbitals may also be important for several reasons: directly through resonance/delocalization, indirectly by the energetics of the system which determines the geometry of the H-bond (which may also be driven in part or fully by resonance), or through inductive effects such as in DHP. In the cases where the H-bond is resonance-assisted, the delocalization of some of the involved LMOs centered on X^b and X^c is evident in the LMO plots and their numerical characterization in terms of atomic hybrids, and it shows up in the shielding and spin–spin coupling contributions of these orbitals, along with contributions from additional LMOs in the π -backbone. The acetic acid dimer (AAD) is an interesting system because it exhibits resonance contributions to the H^a shielding both within the “same unit” LMO set as well as intermolecular. In HSA, there is likewise no backbone π -resonance but the analysis nonetheless identifies resonance within the carboxylate groups to contribute directly to the H^a shielding. However, in both systems the loss of H^a shielding is dominantly driven by a low contribution from the $\sigma(O^c \cdots H^a)$ orbital, and for HSA additionally by a large negative contribution from π_x LP O^b reflecting the increased nucleophilicity of O^b due to the negative charge. The shielding of the proton in the

$N \cdots H \cdots N$ hydrogen bond of the GC DNA base pair indicates only a small net contribution from the π system, which is consistent with the energetic analysis of reference [73]. This hydrogen bond is not assisted by resonance, but orbital interactions in the σ framework play a very important role besides electrostatics.

Based on the results and analysis for our set of samples, the answers to the five questions posed in the Introduction are: 1) Very low shielding, sizable positive $H^a \cdots X^b$ indirect spin–spin coupling, and a comparatively small $X^c \cdots H^a$ spin–spin coupling indicate covalent $H^a \cdots X^b$ interactions and a loss of $X^c \cdots H^a$ covalency relative to a reference without a H-bond. 2) Resonance contributions do show up directly in the analysis of the RAHB systems, but they are relatively small in magnitude compared to contributions from the orbitals in the σ framework. The position of the proton within the H-bond bridge, determined by the overall energetics, is decisive. Our analysis therefore corroborates the previous finding by Alkorta et al.^[82] that the *direct* influence of resonance on the proton’s NMR parameters is small. The authors of reference [83] also concluded that the effect of resonance of the H-bond is indirect, based on an analysis of energies and electron densities at bond critical points. Structure, energetics and NMR parameters are nonetheless linked through the underlying electronic structure. 3) We find important contributions to the proton shielding that can be attributed to resonance, in the sense of electron delocalization, for systems that do not fall into the RAHB category. 4) Similarly strongly de-shielded protons in different compounds do not necessarily imply that the same mechanisms are at play. For instance, some of the shielding contributions are almost transferable between HSA and NMA while others are not, meaning that the two molecules are “similar, yet different” as far as the H^a shielding is concerned. 5) $X \cdots H \cdots X$ environments with $X=O$ and $X=N$ reveal very similar characteristics in the analysis. Bond orders and references for shielding and spin–spin coupling cannot be compared directly among compounds with different X, but when suitable reference compounds are used to compare the computational data then the trends related to the H-bond formation can be compared. Our analysis did not find evidence for resonance contributions to the H^a proton shielding of the GC DNA base pair.

In conclusion, there is much that can be learned about the strength and covalent character of hydrogen bonding from experimental NMR data and comparison with results of ab initio calculations and accompanying analyses in terms of lone-pair and bond LMOs. This work has considered an initial set of molecules with a wide range of proton chemical shifts and H–X spin–spin couplings reflecting the variable strengths and covalency of hydrogen bonds within and across molecules.

Acknowledgements

This research was supported by the National Science Foundation, grant CHE-1265833 (J.A.). G.A.A. acknowledges the Argentine Agency for Promotion of Science and Technology (FONCYT), grant PICT2012-1214. All computations were per-

formed with resources provided by the Center for Computational Research at the University at Buffalo.

Keywords: ab initio calculations · bond theory · computer chemistry · hydrogen bonds · NMR spectroscopy

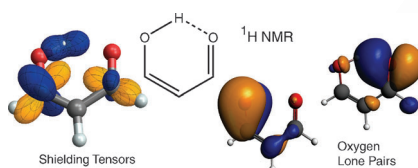
- [1] T. Steiner, *Angew. Chem. Int. Ed.* **2002**, *41*, 48–76; *Angew. Chem.* **2002**, *114*, 50–80.
- [2] S. Grzesiek, F. Cordier, V. Jaravine, M. Barfield, *Prog. Nucl. Magn. Reson. Spectrosc.* **2004**, *45*, 275–300.
- [3] I. Alkorta, J. Elguero, G. S. Denisov, *Magn. Reson. Chem.* **2008**, *46*, 599–624.
- [4] E. Arunan, G. R. Desiraju, R. A. Klein, J. Sadlej, S. Scheiner, I. Alkorta, D. C. Clary, R. H. Crabtree, J. J. Dannenberg, P. Hobza, H. G. Kjaergaard, A. C. Legon, B. Mennucci, D. J. Nesbitt, *Pure Appl. Chem.* **2011**, *83*, 1637–1641.
- [5] E. Arunan, G. R. Desiraju, R. A. Klein, J. Sadlej, S. Scheiner, I. Alkorta, D. C. Clary, R. H. Crabtree, J. J. Dannenberg, P. Hobza, H. G. Kjaergaard, A. C. Legon, B. Mennucci, D. J. Nesbitt, *Pure Appl. Chem.* **2011**, *83*, 1619–1636.
- [6] A. J. Dingley, S. Grzesiek, *J. Am. Chem. Soc.* **1998**, *120*, 8293–8297.
- [7] F. Cordier, M. Rogowski, S. Grzesiek, A. Bax, *J. Magn. Reson.* **1999**, *140*, 510–512.
- [8] M. Pecul, J. Leszczynski, J. Sadlej, *J. Chem. Phys.* **2000**, *112*, 7930–7938.
- [9] H. Benedict, I. G. Shenderovich, O. L. Malkina, V. G. Malkin, G. S. Denisov, N. S. Golubev, H.-H. Limbach, *J. Am. Chem. Soc.* **2000**, *122*, 1979–1988.
- [10] M. Pietrzak, A. C. Try, B. Andrioletti, J. L. Sessler, P. Anzenbacher, H.-H. Limbach, *Angew. Chem. Int. Ed.* **2008**, *47*, 1123–1126; *Angew. Chem.* **2008**, *120*, 1139–1142.
- [11] W. W. Cleland, M. M. Kreevoy, *Science* **1994**, *264*, 1887–1890.
- [12] S. J. Grabowski, *Ann. Rep. Prog. Chem. Sect. C* **2006**, *102*, 131–165.
- [13] S. J. Grabowski, *Chem. Rev.* **2011**, *111*, 2597–2625.
- [14] W. D. Arnold, E. Oldfield, *J. Am. Chem. Soc.* **2000**, *122*, 12835–12841.
- [15] J. D. Roberts, *ABCs of FT-NMR*, University Science Books, Sausalito, **2000**.
- [16] N. Zarycz, G. A. Aucar, C. O. Della Védova, *J. Phys. Chem. A* **2010**, *114*, 7162–7172.
- [17] K. Sutter, J. Autschbach, *J. Am. Chem. Soc.* **2012**, *134*, 13374–13385.
- [18] K. Jackowski, M. Jaszunski, M. Wilczek, *J. Phys. Chem. A* **2010**, *114*, 2471–2475.
- [19] P. Garbacz, K. Jackowski, W. Makulski, R. E. Wasylshen, *J. Phys. Chem. A* **2012**, *116*, 11896–11904.
- [20] L. J. Altman, P. Laungani, G. Gunnarsson, H. Wennerström, S. Forsén, *J. Am. Chem. Soc.* **1978**, *100*, 8264–8266.
- [21] R. L. Lintvedt, H. F. Holtzclaw, *J. Am. Chem. Soc.* **1966**, *88*, 2713–2716.
- [22] K. A. Manbeck, N. C. Boaz, N. C. Bair, A. M. S. Sanders, A. L. Marsh, *J. Chem. Educ.* **2011**, *88*, 1444–1445.
- [23] R. J. Abraham, M. Mobli, *Magn. Reson. Chem.* **2007**, *45*, 865–877.
- [24] J. Guo, P. M. Tolstoy, B. Koeppe, N. S. Golubev, G. S. Denisov, S. N. Smirnov, H.-H. Limbach, *J. Phys. Chem. A* **2012**, *116*, 11180–11188.
- [25] N. A. Friøystein, E. Sletten, *J. Am. Chem. Soc.* **1994**, *116*, 3240–3250.
- [26] D. Ajami, P. M. Tolstoy, H. Dube, S. Odermatt, B. Koeppe, J. Guo, H.-H. Limbach, J. Rebek, *Angew. Chem. Int. Ed.* **2011**, *50*, 528–531; *Angew. Chem.* **2011**, *123*, 548–552.
- [27] H.-H. Limbach, P. M. Tolstoy, N. Pérez-Hernández, J. Guo, I. G. Shenderovich, G. S. Denisov, *Isr. J. Chem.* **2009**, *49*, 199–216.
- [28] P. M. Tolstoy, J. Guo, B. Koeppe, N. S. Golubev, G. S. Denisov, S. N. Smirnov, H.-H. Limbach, *J. Phys. Chem. A* **2010**, *114*, 10775–10782.
- [29] B. Koeppe, J. Guo, P. M. Tolstoy, G. S. Denisov, H.-H. Limbach, *J. Am. Chem. Soc.* **2013**, *135*, 7553–7566.
- [30] I. G. Shenderovich, A. P. Burtsev, G. S. Denisov, N. S. Golubev, H.-H. Limbach, *Magn. Reson. Chem.* **2001**, *39*, S91–S99.
- [31] P. Schah-Mohammedi, I. G. Shenderovich, C. Detering, H.-H. Limbach, P. M. Tolstoy, S. N. Smirnov, G. S. Denisov, N. S. Golubev, *J. Am. Chem. Soc.* **2000**, *122*, 12878–12879.
- [32] H. Benedict, H.-H. Limbach, M. Wehlan, W.-P. Fehlhammer, N. S. Golubev, R. Janoschek, *J. Am. Chem. Soc.* **1998**, *120*, 2939–2950.
- [33] S. N. Smirnov, N. S. Golubev, G. S. Denisov, H. Benedict, P. Schah-Mohammedi, H.-H. Limbach, *J. Am. Chem. Soc.* **1996**, *118*, 4094–4101.
- [34] M. Swart, C. Fonseca Guerra, F. M. Bickelhaupt, *J. Am. Chem. Soc.* **2004**, *126*, 16718–16719.
- [35] G. Gilli, F. Bellucci, V. Ferretti, V. Bertolasi, *J. Am. Chem. Soc.* **1989**, *111*, 1023–1028.
- [36] L. Sobczyk, S. J. Grabowski, T. M. Krygowski, *Chem. Rev.* **2005**, *105*, 3513–3560.
- [37] B. Bankiewicz, P. Matczak, M. Palusiak, *J. Phys. Chem. A* **2012**, *116*, 452–459.
- [38] Y. Mo, *J. Phys. Chem. A* **2012**, *116*, 5240–5246.
- [39] A. Nowroozi, H. Raissi, H. Hajjibadi, P. M. Jahani, *Int. J. Quantum Chem.* **2011**, *111*, 3040–3047.
- [40] F. Weinhold, *Natural Bond Orbital Methods in Encyclopedia of Computational Chemistry* (Ed.: P. von Ragué Schleyer), Wiley, Chichester, **1998**, pp. 1792–1811.
- [41] H. Raissi, M. Yoosefian, A. Hajjizadeh, J. s. Imampour, M. Karimi, F. Farzad, *Bull. Chem. Soc. Jpn.* **2012**, *85*, 87–92.
- [42] C. G. Giribet, M. C. Ruiz de Azúa, *J. Phys. Chem. A* **2012**, *116*, 12175–12183.
- [43] J. Autschbach, *J. Chem. Phys.* **2008**, *128*, 164112–11.
- [44] J. Autschbach, S. Zheng, *Magn. Reson. Chem.* **2008**, *46*, S45–S55.
- [45] J. Autschbach, *J. Chem. Phys.* **2007**, *127*, 124106–11.
- [46] A. E. Hansen, T. D. Bouman, *J. Chem. Phys.* **1985**, *82*, 5035–5047.
- [47] S. Kurtkaya, V. Barone, J. E. Peralta, R. H. Contreras, J. P. Snyder, *J. Am. Chem. Soc.* **2002**, *124*, 9702–9703.
- [48] R. H. Contreras, A. L. Esteban, E. Diez, N. J. Head, E. W. Della, *Mol. Phys.* **2006**, *104*, 485–492.
- [49] N. Zarycz, G. A. Aucar, *J. Chem. Phys.* **2012**, *136*, 174115–10.
- [50] S. Zheng, J. Autschbach, *Chem. Eur. J.* **2011**, *17*, 161–173.
- [51] M. Bühl, F. R. Knight, A. Kristkova, I. Malkin Ondik, O. L. Malkina, R. A. M. Randall, A. M. Z. Slawin, J. D. Woollins, *Angew. Chem. Int. Ed.* **2013**, *52*, 2495–2498; *Angew. Chem.* **2013**, *125*, 2555–2558.
- [52] G. A. Aucar, *Concepts Magn. Reson. A* **2008**, *32*, 88–116.
- [53] Gaussian 09, Revision D.01, M. J. Frisch, G. W. Trucks, J. A. Pople, et al., Gaussian, Inc., Wallingford CT, **2009**; <http://www.gaussian.com/>, accessed May 2015.
- [54] E. J. Baerends, et al., *Amsterdam Density Functional (ADF), 2012 Developers' Version, SCM*, Theoretical Chemistry, Vrije Universiteit, Amsterdam.
- [55] J. P. Perdew, K. Burke, M. Ernzerhof, *Phys. Rev. Lett.* **1996**, *77*, 3865–3868.
- [56] C. Adamo, V. Barone, *J. Chem. Phys.* **1999**, *110*, 6158–6170.
- [57] E. Zurek, C. Pickard, J. Autschbach, *J. Phys. Chem. A* **2009**, *113*, 4117–4124.
- [58] B. C. Mort, J. Autschbach, *J. Am. Chem. Soc.* **2006**, *128*, 10060–10072.
- [59] E. D. Glendening, J. K. Badenhoop, A. E. Reed, J. E. Carpenter, J. A. Bohmann, C. M. Morales, F. Weinhold, *NBO 5.0*, Theoretical chemistry institute, University of Wisconsin, Madison, **2001**; <http://nbo.chem.wisc.edu>, accessed May 2015.
- [60] J. A. Bohmann, F. Weinhold, T. C. Farrar, *J. Chem. Phys.* **1997**, *107*, 1173–1184.
- [61] S. J. Wilkens, W. M. Westler, J. L. Markley, F. Weinhold, *J. Am. Chem. Soc.* **2001**, *123*, 12026–12036.
- [62] K. Wiberg, *Tetrahedron* **1968**, *24*, 1083–1096.
- [63] I. Mayer, *J. Comput. Chem.* **2007**, *28*, 204–221.
- [64] P. E. Hansen, *Magn. Reson. Chem.* **2008**, *46*, 726–729.
- [65] W. H. Richardson, R. F. Steed, *J. Org. Chem.* **1967**, *32*, 771–774.
- [66] M. Bühl, S. Gaemers, C. J. Elsevier, *Chem. Eur. J.* **2000**, *6*, 3272–3280.
- [67] E. Zurek, C. J. Pickard, B. Walczak, J. Autschbach, *J. Phys. Chem. A* **2006**, *110*, 11995–12004.
- [68] H. Fukui, *Magn. Reson. Rev.* **1987**, *11*, 205–274.
- [69] J. B. Grutzner, *Chemical Shift Theory: Orbital Symmetry and Charge Effects on Chemical Shifts, in Recent Advances in Organic NMR Spectroscopy*, Norell, Landisville, **1987**, pp. 17–42.
- [70] R. Wasylshen, *Characterization of NMR Tensors via Experiment and Theory in Calculation of NMR and EPR Parameters: Theory and Applications* (Eds.: M. Kaupp, M. Bühl, V. G. Malkin), Wiley-VCH, Weinheim, **2004**, pp. 433–447.
- [71] D. L. Bryce, R. E. Wasylshen, *J. Am. Chem. Soc.* **2000**, *122*, 3197–3205.
- [72] J. Autschbach, *J. Chem. Educ.* **2012**, *89*, 1032–1040.
- [73] C. Fonseca Guerra, F. M. Bickelhaupt, J. G. Snijders, E. J. Baerends, *Chem. Eur. J.* **1999**, *5*, 3581–3594.

- [74] C. Fonseca Guerra, H. Zijlstra, G. Paragi, F. M. Bickelhaupt, *Chem. Eur. J.* **2011**, *17*, 12612–12622.
- [75] L. Guillaumes, S. Simon, C. Fonseca Guerra, *ChemistryOpen* **2015**, DOI: 10.1002/open.201402132. ■■■please update if possible■■■
- [76] L. P. Wolters, N. W. G. Smits, C. Fonseca Guerra, *Phys. Chem. Chem. Phys.* **2015**, *17*, 1585–1592.
- [77] J. Kowalewski, *Annu. Rep. NMR Spectrosc.* **1982**, *12*, 81–176.
- [78] J. Autschbach, B. Le Guennic, *J. Chem. Educ.* **2007**, *84*, 156–171.
- [79] J. E. Del Bene, I. Alkorta, J. Elguero, *J. Chem. Theory Comput.* **2008**, *4*, 967–973.
- [80] M. A. Watson, P. Salek, P. Macak, M. Jaszunski, T. Helgaker, *Chem. Eur. J.* **2004**, *10*, 4627–4639.
- [81] R. H. Contreras, J. C. Facelli, *Annu. Rep. NMR Spectrosc.* **1993**, *27*, 255–356.
- [82] I. Alkorta, J. Elguero, O. Mó, M. Yáñez, J. E. Del Bene, *Chem. Phys. Lett.* **2005**, *411*, 411–415.
- [83] P. Sanz, O. Mó, M. Yáñez, J. Elguero, *J. Phys. Chem. A* **2007**, *111*, 3585–3591.

Received: June 17, 2015
Published online on ■■■■■, 0000

FULL PAPER

Breaking cover: NMR spectroscopic parameters of the proton involved in hydrogen bonding have been studied theoretically. The analysis results show how NMR spectroscopic parameters that are characteristic for hydrogen bonded protons are influenced by the geometry and degree of covalency of the hydrogen bond as well as intra- and intermolecular resonance (see figure). ■■■ok?■



Computer Chemistry

K. Sutter, G. A. Aucar, J. Autschbach*

■■ - ■■

Analysis of Proton NMR in Hydrogen Bonds in Terms of Lone-Pair and Bond Orbital Contributions

Please check that the ORCID identifiers listed below are correct. We encourage all authors to provide an ORCID identifier for each coauthor. ORCID is a registry that provides researchers with a unique digital identifier. Some funding agencies recommend or even require the inclusion of ORCID IDs in all published articles, and authors should consult their funding agency guidelines for details. Registration is easy and free; for further information, see <http://orcid.org/>.

Kiplangat Sutter
Gustavo A. Aucar
Jochen Autschbach